

Bounded Deep Unfolding for Joint Beamforming and Scheduling in Multi-Cell MIMO Networks

Jiansheng Li, Shuqi Chai, Fan Xu, Kaiming Shen, Guangxu Zhu, Junting Chen

Abstract—This paper investigates the joint resource block group (RBG) scheduling and beamforming optimization problem for weighted sum-rate (WSR) maximization in multi-cell multiple-input multiple-output (MIMO) downlink networks. While the Fast Fractional Programming (FastFP) framework provides a reliable model-driven solution, it suffers from conservative continuous beamforming updates and prohibitive computational overhead during the discrete RBG matching phase. To address these bottlenecks, we propose a joint deep unfolding framework comprising two core modules: P-Net and K-Net. For continuous beamforming, P-Net learns an adaptive relaxation factor along the analytical FastFP update direction. By strictly constraining this factor within an ascent-preserving interval, P-Net accelerates the optimization trajectory while rigorously retaining monotonic improvement and stationary-point convergence guarantees. For discrete RBG scheduling, K-Net learns a long-horizon priority policy that guides a low-complexity greedy assignment, effectively preserving the assignment quality while bypassing the high complexity of Hungarian matching. Both networks leverage analytical algorithmic priors and utilize recurrent parameter sharing, enabling flexible inference beyond the training horizon. Extensive simulations demonstrate that the proposed joint framework achieves higher WSR and faster execution times than conventional model-driven baselines, while generalizing robustly across unseen network scales, antenna configurations, and channel conditions without retraining.

Index Terms—Deep unfolding, fractional programming (FP), joint beamforming and scheduling, multi-cell MIMO, learning-to-optimize.

I. INTRODUCTION

To meet the stringent capacity and connectivity demands of future wireless systems [1], [2], dense spectrum reuse and multi-cell MIMO transmission have emerged as key physical-layer enablers [3], [4]. However, aggressive co-channel reuse severely exacerbates inter-cell and inter-user interference, making interference-aware resource coordination and beamforming crucial for unlocking the full potential of MIMO [5], [6]. In Orthogonal Frequency Division Multiple Access (OFDMA) downlink systems, discrete resource block group (RBG) allocation fundamentally dictates the cross-cell interference topology [7], while continuous beamformers control desired signal power and interference leakage. Consequently, coupling these variables transforms the joint scheduling and beamforming task into a highly complex nonlinear mixed-integer optimization problem [8]–[12].

Jiansheng Li, Kaiming Shen, and Junting Chen are with the School of Science and Engineering, The Chinese University of Hong Kong, Shenzhen, 518172, China (e-mail: jianshengli@link.cuhk.edu.cn; shenkaiming@cuhk.edu.cn; juntingchen@cuhk.edu.cn).

Shuqi Chai and Guangxu Zhu are with the Shenzhen Research Institute of Big Data, Shenzhen 518172, China (e-mail: schai@sribd.cn; gxzhu@sribd.cn).

Fan Xu is with the School of Electronic Information Engineering, Tongji University, Shanghai 201804, China (e-mail: xxiaof999@tongji.edu.cn).

Classical model-driven optimization methods remain the backbone of WSR maximization in wireless networks. For a fixed RBG allocation, the continuous beamforming problem is commonly handled by the weighted minimum mean-square error (WMMSE) algorithm and the fractional programming (FP) framework [13]–[15]. The WMMSE algorithm exploits the equivalence between rate maximization and weighted MSE minimization and solves the resulting problem via block coordinate descent, with provable convergence to a stationary point. However, in multi-cell MIMO networks, each WMMSE iteration typically involves large matrix inversions whose dimensions scale with the number of transmit antennas, and the transmit-power constraints require the search for Lagrange multipliers. These operations can become computationally demanding when massive antenna arrays are deployed. The importance of this complexity bottleneck has also motivated recent efforts to rethink WMMSE, such as reduced-complexity variants that exploit the low-dimensional structure of stationary precoders or recursive per-antenna updates to reduce the antenna-dimensional scaling [16]. FP provides another powerful model-driven approach by applying the Lagrangian dual transform and the quadratic transform to recast SINR-ratio objectives into more tractable surrogate forms [15]. Moreover, WMMSE can be interpreted as a special case of FP, revealing a close connection between these two algorithmic families.

Beyond continuous beamforming and power control, FP has also been extended to discrete wireless scheduling problems, where the transformed objective can induce analytically derived edge utilities for combinatorial matching [17]. Following this line, FP combined with the Hungarian algorithm has been used for downlink multiuser MIMO resource allocation, where beamforming and user/RBG scheduling are alternately optimized [18]. Although FP-Hungarian methods preserve the problem structure and provide exact local solutions, repeatedly executing the matching step is computationally prohibitive. Furthermore, maximizing the current surrogate is locally myopic, as current RBG assignments fundamentally alter subsequent interference topologies and beamforming trajectories. This motivates a learning-guided scheduling mechanism that retains the analytical FP-derived edge utility while bypassing the overhead of repeated Hungarian matching to optimize the long-term trajectory.

Learning-based optimization methods have emerged as a promising way to improve the speed-performance tradeoff of resource allocation algorithms. Early learning-based approaches either approximate the input-output behavior of optimization algorithms or directly learn resource-allocation policies, enabling fast inference once trained [19], [20]. Reinforcement learning has also been applied to radio resource

management and wireless scheduling, where the scheduling process is naturally modeled through states, actions, and rewards [21]. However, directly mapping channel states or queue states to discrete resource-allocation actions may face large combinatorial action spaces, feasibility enforcement difficulties, sample-efficiency issues, and limited interpretability. Learning-to-optimize methods for wireless resource management have therefore emphasized the importance of embedding learning into structured optimization procedures rather than replacing the whole solver with a black-box predictor [22]. Recent graph neural network (GNN)-based resource allocation studies further show that exploiting wireless topology, permutation structure, and local interference relations can improve scalability and generalization [23]–[25].

While the above learning-based resource-allocation studies mainly motivate the discrete scheduling component, a parallel line of research focuses on learning-based beamforming optimization. Early learning-based beamforming methods use neural networks to approximate the solution mapping of optimization algorithms or to directly infer beamformers from channel states, thereby reducing online inference latency once the network is trained [19], [26]. However, purely black-box mappings may provide limited interpretability and do not explicitly preserve the algorithmic structure, feasibility mechanism, or convergence behavior of classical beamforming solvers. Deep unfolding addresses this issue by mapping a finite number of iterations of a model-driven algorithm into a layer-wise trainable architecture, so that the resulting neural network (NN) inherits part of the original optimization structure while introducing learnable degrees of freedom [27].

In MIMO beamforming, many existing unfolded networks are built upon WMMSE-type iterations. For instance, IAIDNN unfolds the WMMSE algorithm for MU-MIMO precoding and introduces trainable parameters to replace high-complexity operations in the forward propagation [28]. Matrix-inverse-free WMMSE further reformulates the WMMSE update to avoid matrix inversion, eigendecomposition, and bisection-type operations, making the resulting iterations more suitable for real-time implementation and deep unfolding [29]. Graph-based unfolded WMMSE methods exploit the interference topology of wireless networks and use graph neural networks to parameterize the unfolded update, thereby improving scalability and generalization across network instances [30]. These studies demonstrate that learning selected components of an iterative beamforming solver can provide a favorable speed-performance tradeoff. Nevertheless, since they are mainly derived from WMMSE-type updates, they may still inherit the structural limitations of the target algorithm, such as complicated power-constraint handling, matrix-related operations, or limited adaptation to multi-cell MIMO settings.

To overcome the inherent structural bottlenecks of WMMSE-based unfolding, recent research has shifted towards the FP framework. DeepFP unfolds FastFP for MIMO beamforming and learns acceleration-related parameters, showing that FP iterations can be improved through data-driven tuning [31]. A core concept in FastFP is the conservative curvature bound, which guarantees monotonic ascent via the minorization-maximization (MM) principle [32], [33]. How-

ever, this conservative bound severely limits the step size in heterogeneous channels, leading to slower convergence rates.

Motivated by this limitation, this paper proposes to learn an adaptive relaxation factor along the analytical FastFP update direction, which can accelerate convergence without overshooting the safe region or violating the monotonic ascent property. Specifically, at each iteration, P-Net utilizes the analytical FastFP guide \mathbf{V}^{FP} and learns an adaptive relaxation factor $\alpha^{(\tau)} \in (0, 2)$ to update the state (which may include Nesterov momentum $\mathbf{U}^{(\tau-1)}$):

$$\mathbf{V}^{(\tau)} = \mathbf{U}^{(\tau-1)} + \alpha^{(\tau)} \left(\mathbf{V}^{\text{FP}} - \mathbf{U}^{(\tau-1)} \right).$$

Constraining $\alpha^{(\tau)}$ ensures that the update strictly remains within the ascent-preserving interval of the quadratic surrogate. Coupled with a low-complexity surrogate safety-check and restart mechanism to handle the non-monotonicity of Nesterov momentum, P-Net significantly accelerates the FastFP trajectory while rigorously preserving the monotonic ascent and stationary-point convergence properties of the MM framework. Thus, instead of allowing the neural network to replace or freely modify the update rule as in DeepFP, our continuous module learns only a bounded relaxation factor along the analytical FastFP direction. This design choice is motivated by a simple principle: the learning module should accelerate the reliable optimizer, rather than destroy the mechanism that makes the optimizer reliable. Such a philosophy is also consistent with recent signal-processing studies showing that analytic structures and a small number of learnable parameters can improve efficiency while retaining theoretical control [34]–[36].

Furthermore, for the discrete allocation phase, we propose K-Net, a policy-guided priority scheduler. Rather than directly predicting assignments, K-Net preserves the analytical FastFP edge metric $\xi_{u,i,n}$ as a physics-informed utility and learns a priority ordering for sequential greedy RBG selection. This ordering-based design effectively avoids repeated Hungarian matching, reducing the allocation complexity from $\mathcal{O}(UK^3)$ to $\mathcal{O}(UK^2)$ (when each user contains $N = K$ logical slots). Trained via terminal WSR feedback, K-Net optimizes the long-term allocation trajectory rather than merely maximizing myopic local surrogates.

The main contributions of this paper are summarized as follows:

- We formulate the joint RBG scheduling and beamforming problem in multi-cell MIMO networks as a mixed-integer WSR maximization problem, explicitly identifying the computational bottlenecks of conventional FP-based continuous updates and discrete matching.
- We develop P-Net to accelerate the continuous beamforming stage. By learning a bounded relaxation factor along the analytical FastFP direction, P-Net expedites convergence while strictly preserving the model-driven structure and the ascent-preserving interval.
- We propose K-Net for discrete RBG scheduling. Rather than predicting the assignment matrix directly, it learns a priority ordering to guide a low-complexity greedy

decoder, significantly reducing allocation overhead while retaining analytical FP priors.

- We establish rigorous monotonic ascent and stationary-point convergence guarantees for the bounded P-Net update. For the Nesterov-accelerated variant, we introduce a low-complexity surrogate safety-check mechanism to strictly preserve these theoretical properties.
- Extensive simulations confirm that the joint P-Net + K-Net framework achieves a superior performance-runtime tradeoff compared to conventional baselines. Furthermore, the proposed models generalize robustly across unseen network scales, antenna dimensions, and channel conditions without retraining.

The remainder of this paper is organized as follows. Section II introduces the multi-cell MIMO system model and formulates the joint RBG allocation and beamforming optimization problem. Section III reviews the traditional fractional programming framework, including the continuous FastFP update and the discrete RBG allocation subproblem. Section IV details the proposed deep unfolding framework, including P-Net for bounded FastFP beamforming acceleration and K-Net for policy-guided RBG scheduling. Section V provides extensive numerical results to evaluate the performance, runtime, and generalization ability of the proposed method. Finally, Section VI concludes the paper.

Throughout this paper, boldface uppercase and lowercase letters denote matrices and vectors, respectively. The space of $M \times N$ complex matrices is denoted by $\mathbb{C}^{M \times N}$. The operators $(\cdot)^T$ and $(\cdot)^H$ stand for the transpose and conjugate transpose of a matrix, respectively. The trace and determinant of a matrix are represented by $\text{Tr}(\cdot)$ and $\det(\cdot)$, respectively. \mathbf{I}_N denotes an $N \times N$ identity matrix. $\Re\{\cdot\}$ extracts the real part of a complex variable. $\mathbb{E}[\cdot]$ denotes the statistical expectation. $\|\cdot\|_F$ represents the Frobenius norm of a matrix. $\mathcal{P}_{\mathcal{W}}(\cdot)$ denotes the projection operator onto a given set \mathcal{W} . For Hermitian matrices \mathbf{A} and \mathbf{B} , $\mathbf{A} \preceq \mathbf{B}$ indicates that $\mathbf{B} - \mathbf{A}$ is positive semi-definite, and $\lambda_{\max}(\mathbf{A})$ denotes the maximum eigenvalue of \mathbf{A} . The cardinality of a set \mathcal{A} is denoted by $|\mathcal{A}|$, and $[N]$ defines the set of integers $\{0, 1, \dots, N - 1\}$.

II. SYSTEM MODEL AND PROBLEM FORMULATION

A. System Model

We consider a downlink MIMO transmission scenario in a multi-cell Multiple-Input Multiple-Output (MIMO) wireless network. The system consists of a set of base stations (BSs), denoted by \mathcal{A} , a set of users, denoted by \mathcal{U} , and a set of shared resource block groups (RBGs), denoted by \mathcal{K} . All BSs operate on a co-channel deployment basis, sharing the entire set of RBGs, which inherently induces inter-cell interference. The cardinalities of these sets are given by $B = |\mathcal{A}|$, $U = |\mathcal{U}|$, and $K = |\mathcal{K}|$. Each BS is equipped with M_t transmit antennas, and each user equipment is equipped with M_r receive antennas. The number of spatial data streams transmitted from the serving BS to user u is denoted by d_u , which is assumed identical across all users to maximize spatial multiplexing. The transmit signal vector for user u is denoted by $\mathbf{s} \in \mathbb{C}^{d_u}$, normalized such that $\mathbb{E}[\mathbf{s}\mathbf{s}^H] = \mathbf{I}_{d_u}$. Let $[K] \triangleq \{0, 1, \dots, K - 1\}$ denote

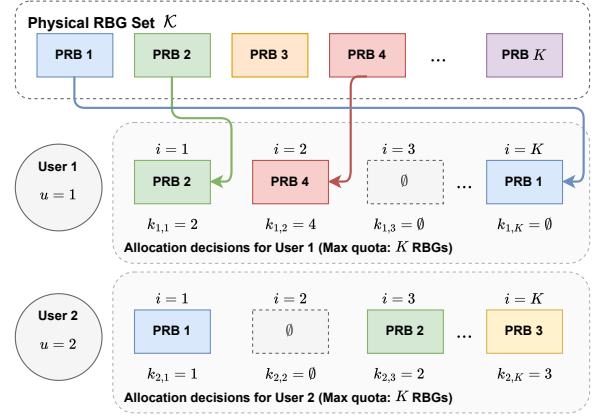


Fig. 1. Illustration of the proposed resource allocation variables. Physical RBG indices (represented as blocks) are directly mapped into predefined logical decision slots for each user. Unused allocation decisions are simply marked with the \emptyset state.

the set of integer from 0 to $K - 1$, which represents the set of RBGs indices. Similarly, $[U]$ denotes the set of user indices.

B. Signal Model and Problem Formulation

To streamline the formulation, we define two decision variables as follows:

- **RBG allocation variable** $k_{u,i} \in [K] \cup \{\emptyset\}$: We introduce a flexible scheduling framework where each user u is granted a quota of N logical allocation decision slots, indexed by $i \in [N]$. Unless otherwise specified, we set $N = K$, so that each user has at most one allocation decision for each physical RBG. The pair (u, i) therefore denotes the i -th allocation decision slot of user u . As illustrated in Fig. 1, $k_{u,i}$ maps this allocation decision slot to a physical RBG index. If $k_{u,i} = \emptyset$, no RBG is allocated to this decision slot; otherwise, $k_{u,i} \in [K]$ and the decision slot becomes active.
- **Transmit beamforming variable** $\mathbf{V}_{b_u, k_{u,i}, u} \in \mathbb{C}^{M_t \times d_u}$: For an active allocation decision slot (u, i) with $k_{u,i} \neq \emptyset$, this precoding matrix is applied by the serving BS b_u to transmit d_u data streams to user u on physical RBG $k_{u,i}$.

We define the set of active allocation decision slots sharing the same physical RBG as (u, i) as

$$\mathcal{C}_{u,i} \triangleq \{(j, \ell) \mid k_{j,\ell} = k_{u,i}, k_{j,\ell} \neq \emptyset\}. \quad (1)$$

For notation brevity, since the serving BS b_u and the assigned RBG $k_{u,i}$ are uniquely determined by the user index u and its decision slot index i , we simplify the comprehensive subscripts $\{b_u, k_{u,i}, u\}$ to $\{u, i\}$ in the sequel.

Therefore, the interference-plus-noise covariance matrix experienced by user u under its active allocation decision (u, i) is given by:

$$\mathbf{M}_{u,i} = \sum_{(j,\ell) \in \mathcal{C}_{-u,i}} \mathbf{H}_{b_j, k_{u,i}, u} \mathbf{V}_{j,\ell} \mathbf{V}_{j,\ell}^H \mathbf{H}_{b_j, k_{u,i}, u}^H + \sigma^2 \mathbf{I}_{M_r}. \quad (2)$$

where $\mathcal{C}_{-u,i} \triangleq \mathcal{C}_{u,i} \setminus \{(u,i)\}$. After that, the achievable rate $R_{u,i}$ for user u on slot i is directly formulated as:

$$R_{u,i} = \log \det (\mathbf{I}_{d_u} + \mathbf{V}_{u,i}^H \mathbf{H}_{u,i}^H \mathbf{M}_{u,i}^{-1} \mathbf{H}_{u,i} \mathbf{V}_{u,i}). \quad (3)$$

Our objective is to maximize the network's Weighted Sum Rate (WSR), where $\rho_u \geq 0$ denotes the priority weight assigned to user u . The joint resource allocation and beamforming optimization problem can be formulated as:

$$\underset{k_{ui}, \mathbf{V}_{u,i}}{\text{maximize}} \quad \sum_{u \in [U]} \rho_u \sum_{i \in [N]} R_{u,i} \quad (4a)$$

$$\text{s.t.} \quad \|\mathbf{V}_{u,i}\|_F^2 \leq P_{\max}, \quad \forall u \in [U], i \in [N] \quad (4b)$$

$$k_{ui} \in [K] \cup \{\emptyset\}, \quad \forall u \in [U], i \in [N] \quad (4c)$$

Constraint (4b) enforces the maximum transmission power P_{\max} for each beamformer. This formulation is a highly non-convex MINLP problem, compounded by the complicated multi-user interference coupling within the log-determinant function. To address problem (4), we first introduce a conventional iterative optimization algorithm in Section III, and subsequently unfold its iterations into a neural network architecture in Section IV to simultaneously accelerate convergence and enhance the achievable system performance.

III. FRACTIONAL PROGRAMMING BASED TRADITIONAL OPTIMIZATION METHODS

To tackle the highly non-convex mixed-integer programming problem in (4), we adopt an alternating optimization (AO) framework to iteratively update the continuous transmit beamforming matrices $\mathbf{V}_{u,i}$ and the discrete RBG allocation variables k_{ui} . Specifically, when fixing the scheduling variables k_{ui} , the continuous beamforming optimization subproblem is tackled via the model-driven Fractional Programming (FP) framework [15]. The core principle is to sequentially decouple the multi-user interference from the desired signal components, thereby transforming the intractable log-determinant objective into a series of analytically tractable quadratic surrogate subproblems. On the other hand, the discrete RBG allocation variables k_{ui} and their associated candidate beamformers $\mathbf{V}_{u,i}$ are jointly evaluated and optimized by exploiting the linear additive properties of the transformed FP objective [17]. This elegant structural decoupling allows the combinatorial assignment task to be partitioned into independent per-user weighted bipartite matching subproblems, which are sequentially and exactly solved via the Hungarian algorithm guided by analytically derived edge utilities.

A. Beamforming Optimization via the FP Framework

To address the matrix ratio terms embedded within the log-determinant operation, we first apply the Lagrangian dual

transform [15]. By introducing an auxiliary variable $\mathbf{\Gamma}_{u,i} \in \mathbb{C}^{d_u \times d_u}$, the original problem is equivalently recast as:

$$\underset{\mathbf{V}, \mathbf{\Gamma}}{\text{max}} \quad \sum_{u,i} \left[\rho_u \log \det (\mathbf{I}_{d_u} + \mathbf{\Gamma}_{u,i}) - \rho_u \text{Tr}(\mathbf{\Gamma}_{u,i}) + \text{Tr} \left(\rho_u \mathbf{V}_{u,i}^H \mathbf{H}_{u,i}^H \mathbf{J}_{u,i}^{-1} \mathbf{H}_{u,i} \mathbf{V}_{u,i} (\mathbf{I}_{d_u} + \mathbf{\Gamma}_{u,i}) \right) \right] \quad (6)$$

where $\mathbf{J}_{u,i} = \mathbf{H}_{u,i} \mathbf{V}_{u,i} \mathbf{V}_{u,i}^H \mathbf{H}_{u,i}^H + \mathbf{M}_{u,i}$ represents the total covariance matrix.

Although (6) successfully isolates the desired signal components, the total covariance matrix $\mathbf{J}_{u,i}$ remains coupled within a matrix inverse. To fully decouple these variables, we apply the Quadratic Transform. By introducing decoding auxiliary variables $\mathbf{Y}_{u,i} \in \mathbb{C}^{M_r \times d_u}$, we establish a quadratic lower bound, yielding the following surrogate problem:

$$\underset{\mathbf{V}, \mathbf{\Gamma}, \mathbf{Y}}{\text{max}} \quad f_{P3}(\mathbf{V}, \mathbf{\Gamma}, \mathbf{Y}), \quad (7)$$

where the explicit expression of f_{P3} is given by (5) at the **bottom of this page**, and

$$\mathbf{\Lambda}_{u,i} \triangleq \rho_u \mathbf{H}_{u,i}^H \mathbf{Y}_{u,i} (\mathbf{I}_{d_u} + \mathbf{\Gamma}_{u,i}). \quad (8)$$

We iteratively update $\mathbf{\Gamma}_{u,i}$, $\mathbf{Y}_{u,i}$, and $\mathbf{V}_{u,i}$ in a block coordinate descent fashion. Based on the first-order optimality conditions, the optimal closed-form updates for the auxiliary variables, when fixing the other variables, are respectively obtained as:

$$\mathbf{\Gamma}_{u,i} = \mathbf{V}_{u,i}^H \mathbf{H}_{u,i}^H \mathbf{M}_{u,i}^{-1} \mathbf{H}_{u,i} \mathbf{V}_{u,i}, \quad (9)$$

$$\mathbf{Y}_{u,i} = \mathbf{J}_{u,i}^{-1} \mathbf{H}_{u,i} \mathbf{V}_{u,i}. \quad (10)$$

When optimizing the transmit beamformers $\mathbf{V}_{u,i}$ with the $\mathbf{\Gamma}_{u,i}$ and $\mathbf{Y}_{u,i}$ fixed, the surrogate function (7) becomes concave with respect to $\mathbf{V}_{u,i}$. Consequently, the optimal closed-form update is given by:

$$\mathbf{V}_{u,i} = (\mathbf{L}_{u,i} + \mu_{u,i} \mathbf{I}_{M_t})^{-1} \mathbf{\Lambda}_{u,i}, \quad (11)$$

where $\mu_{u,i} \geq 0$ is the Lagrange multiplier associated with the power constraint. To express the curvature matrix $\mathbf{L}_{u,i}$ compactly, we define the weighted decoding matrix as:

$$\mathbf{\Psi}_{j,\ell} \triangleq \mathbf{Y}_{j,\ell} (\mathbf{I}_{d_j} + \mathbf{\Gamma}_{j,\ell}) \mathbf{Y}_{j,\ell}^H. \quad (12)$$

Thus, the curvature matrix $\mathbf{L}_{u,i}$ is formulated as:

$$\mathbf{L}_{u,i} = \sum_{(j,\ell) \in \mathcal{C}_{u,i}} \rho_j \mathbf{H}_{b_u, k_{ui}, j}^H \mathbf{\Psi}_{j,\ell} \mathbf{H}_{b_u, k_{ui}, j}. \quad (13)$$

B. FastFP and Nesterov Acceleration

Although the FP framework offers a closed-form solution, computing the inverse of the high-dimensional matrix $\mathbf{L}_{u,i}$ incurs a prohibitive computational complexity of $\mathcal{O}(M_t^3)$, which becomes a critical bottleneck. To circumvent this issue, FastFP [33] leverages the nonhomogeneous bound to construct

$$f_{P3}(\mathbf{V}, \mathbf{\Gamma}, \mathbf{Y}) = \sum_{u,i} \left[\rho_u \log \det (\mathbf{I}_{d_u} + \mathbf{\Gamma}_{u,i}) - \rho_u \text{Tr}(\mathbf{\Gamma}_{u,i}) + \text{Tr} \left(2\Re\{\mathbf{V}_{u,i}^H \mathbf{\Lambda}_{u,i}\} - \rho_u \text{Tr} \left(\mathbf{Y}_{u,i}^H \mathbf{J}_{u,i} \mathbf{Y}_{u,i} (\mathbf{I}_{d_u} + \mathbf{\Gamma}_{u,i}) \right) \right) \right]. \quad (5)$$

a surrogate function that upper-bounds the curvature of the original problem, enabling a closed-form update without matrix inversion.

Lemma 1 (Nonhomogeneous Bound [32]). *For any Hermitian matrix $\mathbf{L} \preceq \mathbf{K}$ and arbitrary matrices \mathbf{V}, \mathbf{Z} of compatible dimensions, the quadratic term is lower-bounded by:*

$$-Tr(\mathbf{V}^H \mathbf{L} \mathbf{V}) \geq -Tr(\mathbf{V}^H \mathbf{K} \mathbf{V}) + 2\Re\{Tr(\mathbf{V}^H (\mathbf{K} - \mathbf{L}) \mathbf{Z})\} - Tr(\mathbf{Z}^H (\mathbf{K} - \mathbf{L}) \mathbf{Z}).$$

By configuring an matrix $\mathbf{K} = \lambda_{u,i} \mathbf{I}_{M_t}$, where $\lambda_{u,i} = \lambda_{\max}(\mathbf{L}_{u,i})$, and subsequently substituting the quadratic term in (7), we obtain the equivalent optimization problem for problem 7:

$$\max_{\mathbf{V}, \mathbf{\Gamma}, \mathbf{Y}, \mathbf{Z}} f_{P4}(\mathbf{V}, \mathbf{\Gamma}, \mathbf{Y}, \mathbf{Z}), \quad (15)$$

where the explicit expression of f_{P4} is given by (14) at the **bottom of this page**.

The auxiliary variable $\mathbf{Z}_{u,i}$ can be optimally updated as $\mathbf{V}_{u,i}^{(\tau-1)}$. Then, the closed-form update for $\mathbf{V}_{u,i}^\tau$ can be computed as:

$$\tilde{\mathbf{V}}_{u,i}^{(\tau)} = \mathbf{V}_{u,i}^{(\tau-1)} + \frac{1}{\lambda_{u,i}} \left(\mathbf{\Lambda}_{u,i} - \mathbf{L}_{u,i} \mathbf{V}_{u,i}^{(\tau-1)} \right). \quad (16)$$

After which, a projection is applied to ensure the power constraint:

$$\mathbf{V}_{u,i}^{(\tau)} = \begin{cases} \tilde{\mathbf{V}}_{u,i}, & \text{if } Tr(\tilde{\mathbf{V}}_{u,i} \tilde{\mathbf{V}}_{u,i}^H) \leq P_{\max}, \\ \sqrt{\frac{P_{\max}}{Tr(\tilde{\mathbf{V}}_{u,i} \tilde{\mathbf{V}}_{u,i}^H)}} \tilde{\mathbf{V}}_{u,i}, & \text{otherwise.} \end{cases} \quad (17)$$

As proved in [33], this closed-form update is mathematically equivalent to a gradient projection operation bounded by the power constraint \mathcal{W} . Building upon this equivalence, the authors in [33] seamlessly integrated Nesterov's Extrapolation strategy to accelerate convergence. The specific procedure consists of two steps:

1) **Nesterov Momentum and Extrapolation:** Calculate the momentum coefficient $\nu^{(\tau-1)} = \max\{\frac{\tau-2}{\tau+1}, 0\}$ and construct the extrapolation anchor:

$$\mathbf{U}_{u,i}^{(\tau-1)} = \mathbf{V}_{u,i}^{(\tau-1)} + \nu^{(\tau-1)} \left(\mathbf{V}_{u,i}^{(\tau-1)} - \mathbf{V}_{u,i}^{(\tau-2)} \right). \quad (18)$$

2) **Gradient Step with projection:** Compute the unconstrained gradient with $\lambda_{u,n} = \lambda_{\max}(\mathbf{L}_{u,n})$, and restrict it to the feasible set:

$$\mathbf{V}_{u,i}^{(\tau)} = \mathcal{P}_{\mathcal{W}} \left(\mathbf{U}_{u,i}^{(\tau-1)} + \frac{1}{\lambda_{u,i}} \left(\mathbf{\Lambda}_{u,i} - \mathbf{L}_{u,i} \mathbf{U}_{u,i}^{(\tau-1)} \right) \right). \quad (19)$$

where $\mathcal{P}_{\mathcal{W}}(\cdot)$ denotes the projection operation of (17).

To provide a holistic view, the standard FP, along with the unified FastFP and Nesterov FastFP procedures, are summarized in Algorithm 1.

Algorithm 1 Standard FP, FastFP, and Nesterov-FastFP

- 1: **input:** CSI \mathbf{H}
 - 2: Initialize \mathbf{V} satisfying the power constraint and Fixed RBG allocation \mathbf{k}
 - 3: **repeat**
 - 4: Calculate $\mathbf{\Gamma}_{u,i}$ by (9) and $\mathbf{Y}_{u,i}$ by (10).
 - 5: **if** use Standard FP **then**
 - 6: Calculate $\mathbf{V}_{u,i}$ by (11).
 - 7: **else**
 - 8: Set momentum $\nu^{(\tau-1)} = \max\{\frac{\tau-2}{\tau+1}, 0\}$ for Nesterov strategy, or 0 for FastFP.
 - 9: Calculate $\mathbf{U}_{u,i}$ by (18) and $\mathbf{V}_{u,i}$ by (19).
 - 10: **end if**
 - 11: **until** the objective (4) converges
 - 12: **output:** Final converged \mathbf{V}
-

C. RBG Allocation Optimization via Bipartite Matching

The core challenge of RBG allocation lies in its discrete nature, which fundamentally dictates the multi-user interference topology and heavily couples the achievable rates across the network. To address this, we optimize the discrete allocation variables k_{ui} using the equivalent quadratic surrogate problem (15). Given the fixed auxiliary variables ($\mathbf{\Gamma}_{u,i}$ and $\mathbf{Y}_{u,i}$), the FP framework mathematically decouples the complex multi-user interference into a linear additive form. Leveraging this property, we can quantify the potential WSR gain of each candidate slot-to-RBG assignment as an edge weight, thereby transforming the combinatorial resource allocation into a weighted bipartite matching problem [17].

At iteration τ , we evaluate the potential WSR gain of assigning physical RBG n to user u 's i -th decision slot by defining an edge matching weight $\xi_{u,i,n}^{(\tau)}$. This weight is explicitly derived by extracting the terms associated with the candidate beamformer from the surrogate objective (14).

First, we define the set of active allocation decisions from other users currently occupying RBG n as:

$$\mathcal{S}_{-u,n}^{(\tau-1)} \triangleq \{(j, \ell) \mid j \neq u, k_{j,\ell}^{(\tau-1)} = n\}. \quad (20)$$

Consequently, the receiver-side allocation decisions affected by the candidate beamformer are collected in $\mathcal{R}_{u,i,n}^{(\tau)} \triangleq \{(u, i)\} \cup \mathcal{S}_{-u,n}^{(\tau-1)}$. The edge weight $\xi_{u,i,n}^{(\tau)}$ is then formulated as:

$$\begin{aligned} \xi_{u,i,n}^{(\tau)} = & 2\Re \left\{ Tr \left(\hat{\mathbf{V}}_{u,i,n}^{(\tau)H} \mathbf{\Lambda}_{u,i,n}^{(\tau)} \right) \right\} - Tr \left(\hat{\mathbf{V}}_{u,i,n}^{(\tau)H} \mathbf{L}_{u,i,n} \hat{\mathbf{V}}_{u,i,n}^{(\tau)} \right) \\ & - \sum_{(j,\ell) \in \mathcal{S}_{-u,n}^{(\tau-1)}} \rho_u Tr \left(\mathbf{V}_{j,\ell}^{(\tau-1)H} \mathbf{H}_{b_j,n,u}^H \mathbf{\Psi}_{u,i}^{(\tau)} \mathbf{H}_{b_j,n,u} \mathbf{V}_{j,\ell}^{(\tau-1)} \right), \end{aligned} \quad (21)$$

$$\begin{aligned} f_{P4} = & \sum_{u,i} \left[\rho_u \log \det(\mathbf{I}_{d_u} + \mathbf{\Gamma}_{u,i}) - \rho_u Tr(\mathbf{\Gamma}_{u,i}) - \rho_u \sigma^2 Tr(\mathbf{Y}_{u,i}^H \mathbf{Y}_{u,i} (\mathbf{I}_{d_u} + \mathbf{\Gamma}_{u,i})) - \lambda_{u,i} Tr(\mathbf{V}_{u,i}^H \mathbf{V}_{u,i}) \right. \\ & \left. + Tr(2\Re \{ \mathbf{V}_{u,i}^H \mathbf{\Lambda}_{u,i} + \mathbf{V}_{u,i}^H (\lambda_{u,i} \mathbf{I}_{M_t} - \mathbf{L}_{u,i}) \mathbf{Z}_{u,i} \}) - Tr(\mathbf{Z}_{u,i}^H (\lambda_{u,i} \mathbf{I}_{M_t} - \mathbf{L}_{u,i}) \mathbf{Z}_{u,i}) \right]. \end{aligned} \quad (14)$$

where the optimal candidate beamformer $\widehat{\mathbf{V}}_{u,i,n}^{(\tau)}$ is given by:

$$\widehat{\mathbf{V}}_{u,i,n}^{(\tau)} = \mathcal{P}_{\mathcal{W}} \left(\mathbf{V}_{u,i}^{(\tau-1)} + \frac{1}{\lambda_{u,i,n}^{(\tau)}} \left(\mathbf{\Lambda}_{u,i,n}^{(\tau)} - \mathbf{L}_{u,i,n}^{(\tau)} \mathbf{V}_{u,i}^{(\tau-1)} \right) \right). \quad (22)$$

The constituent matrices $\mathbf{\Lambda}_{u,i,n}^{(\tau)}$ and $\mathbf{L}_{u,i,n}^{(\tau)}$ are defined as:

$$\mathbf{\Lambda}_{u,i,n}^{(\tau)} = \rho_u \mathbf{H}_{b_u,n,u}^H \mathbf{Y}_{u,i}^{(\tau)} (\mathbf{I}_{d_u} + \mathbf{\Gamma}_{u,i}^{(\tau)}), \quad (23a)$$

$$\mathbf{L}_{u,i,n}^{(\tau)} = \sum_{(j,\ell) \in \mathcal{R}_{u,i,n}^{(\tau)}} \rho_j \mathbf{H}_{b_u,n,j}^H \mathbf{\Psi}_{j,\ell}^{(\tau)} \mathbf{H}_{b_u,n,j}. \quad (23b)$$

As shown in (21), this edge weight captures three critical components: the desired signal contribution of the candidate link, the interference leakage to the receiver-side links in $\mathcal{R}_{u,i,n}^{(\tau)}$, and the interference received from existing transmitters on RBG n .

With the edge weights analytically established, the combinatorial allocation problem becomes a maximum-weight bipartite matching problem. Since our system allows spatial sharing of physical RBGs, the global allocation decouples into U independent per-user matching subproblems. For each user u , a bipartite graph connects its N logical decision slots to the K physical RBGs. The optimal discrete assignment $x_{u,i,n}^* \in \{0, 1\}$ is obtained by solving the following integer linear program via the Hungarian algorithm:

$$\underset{x_{u,i,n} \in \{0,1\}}{\text{maximize}} \quad \sum_{i \in [N]} \sum_{n \in [K]} \xi_{u,i,n}^{(\tau)} x_{u,i,n} \quad (24a)$$

$$\text{s.t.} \quad \sum_{n \in [K]} x_{u,i,n} \leq 1, \quad \forall i \in [N] \quad (24b)$$

$$\sum_{i \in [N]} x_{u,i,n} \leq 1, \quad \forall n \in [K] \quad (24c)$$

Upon obtaining the optimal binary assignment $x_{u,i,n}^*$, the specific RBG index k_{ui} allocated to user u 's i -th decision slot is recovered by:

$$k_{ui} = \begin{cases} n, & \text{if } x_{u,i,n}^* = 1 \text{ and } \xi_{u,i,n}^{(\tau)} > 0, \\ \emptyset, & \text{otherwise.} \end{cases} \quad (25)$$

The overall alternating procedure for joint RBG allocation and continuous beamforming is summarized in Algorithm 2.

Although the FP-based method provides monotonic convergence, addressing real-time MIMO optimization reveals two significant efficiency bottlenecks: 1) *Conservative continuous updates*: Gradient steps guided by the worst-case spectral radius λ_{\max} are overly conservative, resulting in slow convergence for the beamforming variables. 2) *Prohibitive alternating overhead*: In the discrete RBG allocation phase, while formulating candidate edge weights inherently requires matrix operations, the fundamental scaling bottleneck lies in finding the exact optimal assignment. Specifically, applying the Hungarian algorithm demands a prohibitive combinatorial complexity of $\mathcal{O}(UK^3)$ (assuming $N = K$). Repeatedly executing this matching step within the alternating optimization loop renders the traditional framework practically infeasible for large-scale networks.

Algorithm 2 Joint Beamforming Optimization and RBG Allocation via Bipartite Matching

- 1: **input**: Channel matrices \mathbf{H} .
 - 2: **initialize**: Beamforming matrices $\mathbf{V}^{(0)}$ satisfying power constraints, and RBG allocation $\mathbf{k}^{(0)}$.
 - 3: **repeat**
 - 4: **[Beamforming Optimization Step]** *At iteration τ*
 - 5: Update $\mathbf{\Gamma}^{(\tau)}$ and $\mathbf{Y}^{(\tau)}$ via (9) and (10).
 - 6: Update $\mathbf{V}^{(\tau)}$ via (16).
 - 7: **[RBG Allocation Optimization Step]**
 - 8: **for** each user $u \in [U]$ **do**
 - 9: Compute $\Xi_u^{(\tau)} = [\xi_{u,i,n}^{(\tau)}]_{N \times K}$ via (21), $\forall i \in [N], n \in [K]$.
 - 10: Solve (24) via Hungarian algorithm to obtain binary assignment $x_{u,i,n}^*$.
 - 11: Recover $k_{ui}^{(\tau)}$ and update $\mathbf{V}_{u,i}^{(\tau)} \leftarrow \widehat{\mathbf{V}}_{u,i,k_{ui}^{(\tau)}}^{(\tau)}, \forall i \in [N]$.
 - 12: **end for**
 - 13: **until** the objective WSR (4) converges
 - 14: **output**: Final RBG allocation \mathbf{k}^* and beamforming \mathbf{V}^* .
-

IV. BOUNDED DEEP UNFOLDING NETWORK ARCHITECTURE

To overcome the efficiency bottlenecks of the traditional FP framework, we propose a bounded deep unfolding architecture comprising two modules: P-Net and K-Net. A fundamental limitation of conventional AO is its strict reliance on myopic, local surrogate maximization at each iteration. In contrast, P-Net and K-Net share a unified design motivation: they leverage analytical algorithmic priors to guide variable updates from a global optimization trajectory perspective. Specifically, to address the conservative continuous updates, P-Net learns an adaptive, theoretically bounded relaxation factor that accelerates the FastFP beamforming trajectory while rigorously preserving the monotonically non-decreasing property. Concurrently, to tackle the prohibitive combinatorial overhead, K-Net learns a long-horizon priority policy to guide a sequential greedy assignment. This strategically reduces the exact matching complexity from $\mathcal{O}(UK^3)$ to $\mathcal{O}(UK^2)$, allowing the network to directly optimize the long-term allocation trajectory rather than just the immediate local surrogate. Ultimately, the proposed hybrid deep unfolding paradigm substantially reduces the computational time without compromising the optimization performance.

A. P-Net: Bounded Relaxation Controller for Beamforming

1) *Learned Update Rule and its Principle*: A fundamental limitation of the conventional FastFP algorithm is its greedy algorithmic nature: at each iteration τ , it strictly advances toward the exact peak of the current local surrogate function. While anchoring the update exactly at this surrogate maximum guarantees the maximum local elevation of the objective value, it is inherently short-sighted and lacks a global perspective of the entire optimization trajectory. To overcome this limitation, we do not discard the reliable FastFP mathematical framework;

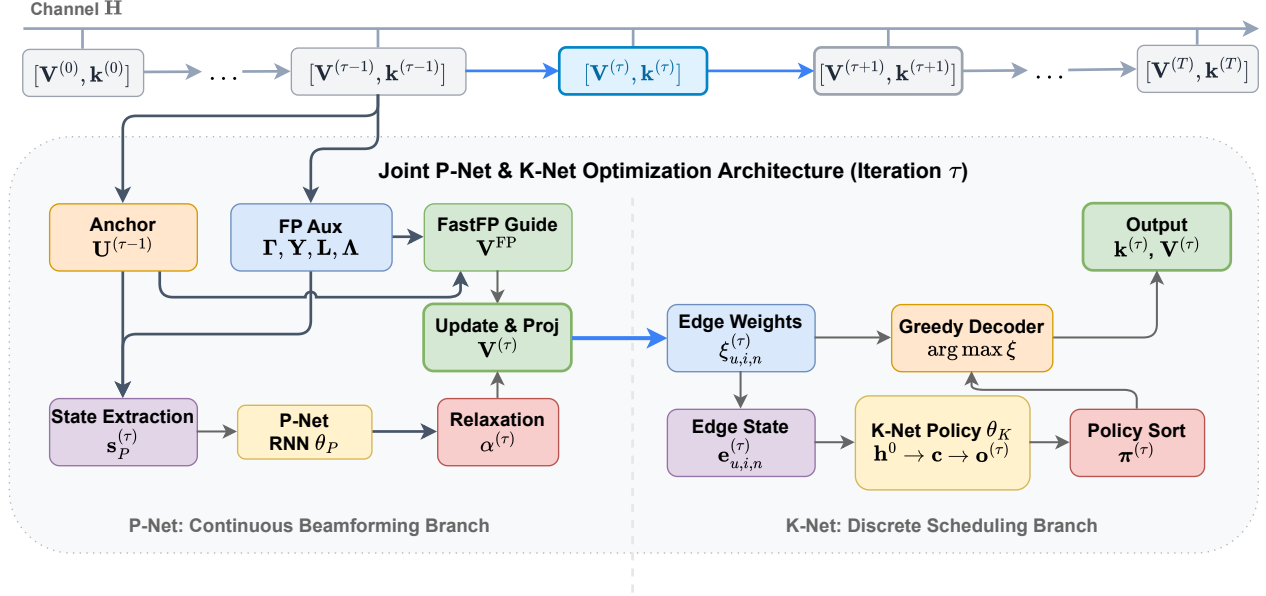


Fig. 2. Algorithmic architecture of the proposed joint P-Net and K-Net deep unfolding framework. The top timeline illustrates the optimization trajectory across shared unrolled layers. Within each iteration τ , the framework executes a sequential bipartite update: First, the continuous branch (P-Net) adaptively accelerates the analytical FastFP beamforming update via a learned relaxation factor $\alpha^{(\tau)}$, bounded strictly within $(0, 2)$ to guarantee monotonic ascent. Second, the newly beamformers $\mathbf{V}^{(\tau)}$ cascade into the discrete branch (K-Net) to formulate the exact matching weights $\xi_{u,i,n}^{(\tau)}$. Driven by these physics-informed edge utilities, K-Net extracts local optimization states and predicts a priority policy $\pi^{(\tau)}$ to guide a low-complexity greedy decoder, ultimately yielding the updated RBG allocation $\mathbf{k}^{(\tau)}$.

rather, we geometrically exploit its local surrogate to design a parameterized update rule.

Specifically, within the FastFP framework, the objective function in problem 15 at an arbitrary τ -th iteration can be interpreted as maximizing a minorant surrogate function:

$$Q(\mathbf{V} | \mathbf{V}^{(\tau-1)}) = 2\Re\{\text{Tr}(\mathbf{V}^H \Xi)\} - \lambda \text{Tr}(\mathbf{V}^H \mathbf{V}) + C^{(\tau-1)}, \quad (26)$$

where $\Xi \triangleq \mathbf{\Lambda} + (\lambda \mathbf{I}_{M_t} - \mathbf{L}) \mathbf{V}^{(\tau-1)}$ denotes the gradient direction matrix. The constant term $C^{(\tau-1)}$, which is independent of \mathbf{V} , is explicitly given by:

$$\begin{aligned} C^{(\tau-1)} = & \rho_u \log \det(\mathbf{I}_{d_u} + \mathbf{\Gamma}_{u,i}^{(\tau-1)}) - \rho_u \text{Tr}(\mathbf{\Gamma}_{u,i}^{(\tau-1)}) \\ & - \rho_u \sigma^2 \text{Tr} \left((\mathbf{Y}_{u,i}^{(\tau-1)})^H \mathbf{Y}_{u,i}^{(\tau-1)} (\mathbf{I}_{d_u} + \mathbf{\Gamma}_{u,i}^{(\tau-1)}) \right) \\ & - \text{Tr} \left((\mathbf{V}^{(\tau-1)})^H (\lambda \mathbf{I}_{M_t} - \mathbf{L}) \mathbf{V}^{(\tau-1)} \right). \end{aligned} \quad (27)$$

Crucially, by replacing the dense quadratic penalty with the scaled identity matrix structure $-\lambda \text{Tr}(\mathbf{V}^H \mathbf{V})$, the surrogate function $Q(\mathbf{V} | \mathbf{V}^{(\tau-1)})$ geometrically forms an *isotropic multi-dimensional paraboloid*.

Instead of myopically restricting the update to the local surrogate maximizer, denoted as $\mathbf{V}^{\text{FP}} = \frac{1}{\lambda} \Xi$, P-Net introduces a NN-guided relaxation factor to capture long-term iterative dependencies. The relaxed update strategy is formulated as:

$$\mathbf{V}^{(\tau)}(\alpha) = \mathbf{V}^{(\tau-1)} + \alpha(\mathbf{V}^{\text{FP}} - \mathbf{V}^{(\tau-1)}), \quad (28)$$

where α is a dynamically learned relaxation factor generated by the NN. This strategy grants the network the flexibility to

explore iteration points either closer to or further beyond the local optimum \mathbf{V}^{FP} along the gradient direction.

2) *Monotonic Increase and Convergence Guarantee*: Let $f(\mathbf{V}^\tau)$ denote the original WSR objective function in problem (4) at τ -th iteration. The following lemma establishes the monotonic ascent property of the proposed update rule in (28).

Lemma 2. *For any relaxation factor $\alpha_{u,i}^{(\tau)} \in (0, 2)$, the sequence of objective values generated by the proposed beamforming update rule in (28) is monotonically non-decreasing, i.e., $f(\mathbf{V}^{(\tau)}) \geq f(\mathbf{V}^{(\tau-1)})$.*

A simple geometric illustration for intuitive understanding is provided in Fig. 3, while the detailed mathematical proof is deferred to Appendix A.

Building upon Lemma 1, the following theorem guarantees that the inference procedure in the algorithm 3 converges to a stationary point.

Theorem 1. *Given a fixed RBG allocation \mathbf{k} , the sequence of beamformers $\{\mathbf{V}^{(\tau)}\}$ generated by the inference procedure in the algorithm 3 converges to a stationary point of the optimization problem in (4).*

The detailed proof is provided in Appendix B. By strictly constraining the learnable relaxation factor within the ascent-preserving interval, the proposed unfolding framework successfully decouples the pursuit of acceleration from the risk of divergence.

3) *P-Net with Nesterov Acceleration*: Building upon the standard FastFP-based P-Net, the incorporation of Nesterov's acceleration is straightforward. The learned update rule is

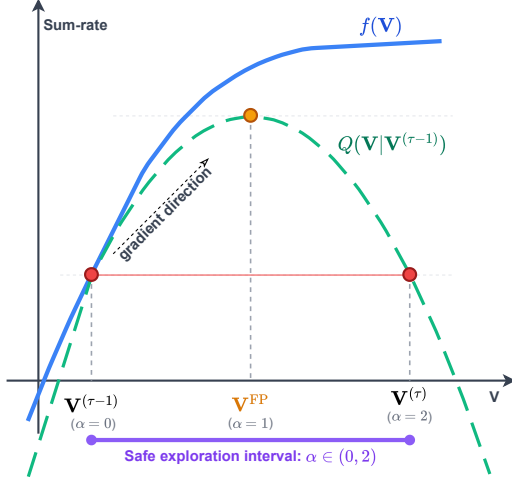


Fig. 3. Geometric illustration of the monotonic ascent guarantee. The surrogate function Q acts as a strict minorant to the true non-convex objective f . While standard FastFP conservatively stops at the local peak ($\alpha = 1$), the proposed P-Net can explore along the gradient direction. Due to the parabola's symmetry, any learned relaxation factor $\alpha \in (0, 2)$ ensures that Q remains above its starting elevation.

naturally extended by replacing the previous state $\mathbf{V}^{(\tau-1)}$ with the extrapolated anchor $\mathbf{U}^{(\tau-1)}$ defined in (18). Consequently, the target FastFP guide \mathbf{V}^{FP} is evaluated at $\mathbf{U}^{(\tau-1)}$ using (18), and the update rule is reformulated as follows:

$$\mathbf{V}^{(\tau)}(\alpha) = \mathbf{U}^{(\tau-1)} + \alpha \left(\mathbf{V}^{\text{FP}} - \mathbf{U}^{(\tau-1)} \right). \quad (29)$$

However, directly applying Nesterov momentum inherently breaks the monotonic non-decreasing property of the FastFP method. To strictly maintain the theoretical guarantees, we introduce a low-complexity *Surrogate Safety Check and Restart* mechanism. Specifically, at τ -th iteration, we first compute a candidate beamformer $\mathbf{V}_{\text{cand}}^{(\tau)}$ guided by the Nesterov anchor $\mathbf{U}^{(\tau-1)}$. We then evaluate the low-complexity surrogate function f_{P3} to compare the candidate against the previous state. If $f_{P3}(\mathbf{V}_{\text{cand}}^{(\tau)}) \geq f_{P3}(\mathbf{V}^{(\tau-1)})$, the momentum step is deemed beneficial and the update is accepted. Otherwise, an unsafe trajectory is detected, triggering a restart: the momentum is discarded ($\mathbf{U}^{(\tau-1)} \leftarrow \mathbf{V}^{(\tau-1)}$), and the network performs a fallback update purely based on the monotonic base point. Since the computation of f_{P3} only involves low-complexity trace operations, and the P-Net inference relies on highly parallelizable lightweight matrix multiplications, the occasional extra forward pass incurs negligible overhead.

Consequently, the monotonic non-decreasing property and the stationary-point convergence guarantees, as established in Lemma 2 and Theorem 1, remain valid for the P-Net equipped with Nesterov acceleration.

4) *Input Feature and Network Architecture*: To avoid excessive physical features and dimensionality explosion, we construct the input state of P-Net using an optimization-state-based feature vector. The network should learn the relaxation policy directly from the local optimization geometry, constraint activity, and acceleration history.

For any active link serving user u on slot i at iteration τ , we define the FastFP update direction and the Nesterov momentum direction as $\mathbf{D}_{u,i}^{(\tau)} = \mathbf{V}_{u,i}^{\text{FP}} - \mathbf{U}_{u,i}^{(\tau-1)}$ and $\mathbf{M}_{u,i}^{(\tau)} = \mathbf{U}_{u,i}^{(\tau-1)} - \mathbf{V}_{u,i}^{(\tau-1)}$, respectively. The six-dimensional compact input feature vector $\mathbf{s}_{u,i}^{(\tau)}$ is constructed entirely from quantities already available during the standard FastFP update:

$$\mathbf{s}_{u,i}^{(\tau)} = [s_1, s_2, s_3, s_4, s_5, s_6]. \quad (30)$$

These six features sequentially correspond to:

- *Update magnitude* ($s_1 = \frac{\|\mathbf{D}_{u,i}^{(\tau)}\|_F}{\|\mathbf{U}_{u,i}^{(\tau-1)}\|_F}$): captures the relative step size of the current FastFP guide.
- *Curvature tightness* ($s_2 = \frac{\text{Tr}(\mathbf{L}_{u,i})/M_i}{\lambda_{u,i}}$): evaluates whether the worst-case majorization bound is overly conservative.
- *Power occupation* ($s_3 = \frac{\|\mathbf{U}_{u,i}^{(\tau-1)}\|_F^2}{P_{\max}}$): indicates the proximity to the feasible power boundary.
- *Projection risk* ($s_4 = \max\left(0, \frac{\|\mathbf{V}_{u,i}^{\text{FP}}\|_F^2}{P_{\max}} - 1\right)$): assesses the likelihood of the candidate being truncated by the power projection.
- *Momentum consistency* ($s_5 = \frac{\Re\{\text{Tr}((\mathbf{D}_{u,i}^{(\tau)})^H \mathbf{M}_{u,i}^{(\tau)})\}}{\|\mathbf{D}_{u,i}^{(\tau)}\|_F \|\mathbf{M}_{u,i}^{(\tau)}\|_F}$): measures the alignment between the Nesterov momentum and the current gradient direction to determine momentum reliability.
- *Iteration stage* ($s_6 = \frac{\tau}{\tau+c}$): allows the network to distinguish between early-stage exploration and late-stage refinement via a bounded scale constant $c > 0$.

Unlike conventional deep unfolding architectures that allocate independent trainable parameters for each layer, the proposed P-Net employs a strict parameter-sharing mechanism parameterized by a recurrent neural network (RNN) \mathcal{F}_θ . The forward pass operates in an autoregressive manner:

$$\begin{cases} \alpha_{u,i}^{(\tau)} = 2 \cdot \text{Sigmoid}\left(\mathcal{F}_\theta\left(\mathbf{s}_{u,i}^{(\tau)}, \mathbf{h}_{u,i}^{(\tau-1)}\right)\right) \\ \mathbf{V}^{(\tau)} = \Psi\left(\mathbf{U}^{(\tau-1)}, \alpha_{u,i}^{(\tau)}\right) \end{cases}, \quad \forall \tau \in [1, T] \quad (31)$$

where $\mathbf{h}_{u,i}^{(\tau-1)}$ represents the hidden state of the RNN, and $\Psi(\cdot)$ denotes the update rule defined in (29). Notably, the Sigmoid(\cdot) activation inherently constrains the network output to the interval $(0, 1)$; hence, the scaling factor of 2 strictly bounds the learned relaxation factor $\alpha_{u,i}^{(\tau)}$ within $(0, 2)$. This guarantees rigorous mathematical compliance with the ascent-preserving interval established in Lemma 2.

The overall unfolded architecture of the proposed P-Net and the detailed computation graph of the τ -th iteration are illustrated in the left side of Fig. 2. This shared-weight design forces the network to learn a generalized, iteration-invariant mapping rather than layer-specific behaviors, significantly reducing the memory footprint. More importantly, it decouples the inference horizon from the training depth T , allowing the algorithm to flexibly extend the iterations until convergence during practical deployment.

5) *Training Strategy*: The training objective is to maximize the Weighted Sum Rate (WSR) across all users. Therefore, the

loss function $\mathcal{L}(\theta)$ over the training dataset \mathcal{D} is defined as the negative expectation of the WSR:

$$\mathcal{L}(\theta) = - \mathbb{E}_{(\mathbf{H}, \mathbf{V}, \mathbf{k}) \sim \mathcal{D}} \left[\sum_{u \in [U]} \rho_u \sum_{i \in [N]} R_{u,i}^{(T)}(\theta) \right], \quad (32)$$

where $R_{u,i}^{(T)}(\theta)$ is the achievable rate evaluated using the beamforming matrices $\mathbf{V}^{(T)}$ output by the final T -th iteration of the unfolded network.

To mitigate memory overhead and prevent vanishing gradients over a long unfolding horizon, we train the recurrent optimizer using Truncated Backpropagation Through Time (TBPTT). Specifically, the T -iteration forward rollout is partitioned into consecutive chunks of length l . During the forward pass, optimization variables and recurrent hidden states are propagated across the entire trajectory. However, during backpropagation, the computational graph is detached at chunk boundaries, thereby restricting gradient flow to local l -step windows.

The end-to-end training and autoregressive inference procedures are summarized in Algorithm 3. For each mini-batch, the beamformers are initialized to satisfy the power constraints. At each iteration $\tau \in [1, T]$, local features $\mathbf{s}_{u,i}^{(\tau)}$ are analytically extracted and fed into P-Net to output $\alpha^{(\tau)}$ and calculate the updated beamformer $\mathbf{V}^{(\tau)}$. After the full rollout, the final loss $\mathcal{L}(\theta)$ is evaluated, and the shared parameters θ are updated via TBPTT.

B. K-Net: Policy-Guided Priority RBG Scheduling

The proposed K-Net is introduced to improve the RBG allocation trajectory over a fixed unfolding horizon. In the AO-based algorithm proposed in Section III, the RBG assignment at iteration τ is obtained by solving a weighted bipartite matching problem to maximize a local surrogate objective, denoted as $\mathcal{Q}^{(\tau)}(\mathbf{k})$. The optimal local assignment via the Hungarian algorithm is given by:

$$\mathbf{k}_{\text{HM}}^{(\tau)} = \arg \max_{\mathbf{k} \in \mathcal{K}_{\text{feas}}} \mathcal{Q}^{(\tau)}(\mathbf{k}), \quad (33)$$

where $\mathcal{K}_{\text{feas}}$ denotes the feasible RBG allocation set.

Similar to the limitation of the FP framework for updating the beamformers, this myopic update ignores the long-term impact of current decisions. Since the current RBG pattern fundamentally alters the subsequent interference topology, auxiliary variables, and beamforming trajectories, maximizing the local surrogate is generally suboptimal for the terminal weighted sum-rate (WSR) under a finite iteration budget T . Specifically, the local maximizer typically diverges from the trajectory-optimal decision:

$$\arg \max_{\mathbf{k}} \mathcal{Q}^{(\tau)}(\mathbf{k}) \neq \arg \max_{\mathbf{k}} \mathbb{E}[F(\mathbf{V}^{(T)}, \mathbf{k}^{(T)}) \mid \mathbf{x}^{(\tau)}, \mathbf{k}], \quad (34)$$

where $F(\cdot)$ denotes the terminal WSR, $\mathbf{x}^{(\tau)}$ represents the complete algorithmic state at iteration τ , and the expectation is conditioned on the current assignment choice $\mathbf{k}^{(\tau)} = \mathbf{k}$.

To bridge this gap, K-Net is designed to learn a long-horizon scheduling policy while preserving the analytical structure of the FastFP assignment subproblem. Instead of replacing the

Algorithm 3 Bounded P-Net Training and Auto-regressive Inference Procedure

- 1: **[Phase 1: Training procedure]**
 - 2: **input:** Training dataset \mathcal{D} , unrolling depth T .
 - 3: Initialize shared network parameters θ .
 - 4: **repeat**
 - 5: Sample mini-batch $\mathbf{H} \sim \mathcal{D}$ and initialize $\mathbf{V}^{(0)}, \mathbf{k}^{(0)}$.
 - 6: **for** $\tau = 1, \dots, T$ **do**
 - 7: Update $\mathbf{\Gamma}_{u,i}^{(\tau)}$ and $\mathbf{Y}_{u,i}^{(\tau)}$ via (9) and (10).
 - 8: Extract $\mathbf{s}_{u,i}^{(\tau)}$ and predict $\alpha_{u,i}^{(\tau)}$ via P-Net \mathcal{F}_θ .
 - 9: Update $\mathbf{V}_{u,n}^{(\tau)}$ via (29) and projection (17).
 - 10: **end for**
 - 11: Compute negative WSR loss $\mathcal{L}(\theta)$ using $\mathbf{V}^{(T)}$.
 - 12: Update shared parameters θ via Truncated BPTT.
 - 13: **until** training loss converges
 - 14: **output:** Trained network parameters θ^* .
 - 15: **[Phase 2: Inference procedure]**
 - 16: **input:** CSI \mathbf{H} , Initialized $\mathbf{V}^{(0)}, \mathbf{k}^{(0)}$, max iterations T_{inf} .
 - 17: **repeat**
 - 18: Update $\mathbf{\Gamma}_{u,i}^{(\tau)}$ and $\mathbf{Y}_{u,i}^{(\tau)}$ via (9) and (10).
 - 19: Extract $\mathbf{s}_{u,i}^{(\tau)}$, predict $\alpha_{u,i}^{(\tau)}$ via \mathcal{F}_{θ^*} , and calculate $\mathbf{V}_{\text{cand}}^{(\tau)}$.
 - 20: **if** $f_{\text{P3}}(\mathbf{V}_{\text{cand}}^{(\tau)}) \geq f_{\text{P3}}(\mathbf{V}^{(\tau-1)})$ **then**
 - 21: $\mathbf{V}_{u,n}^{(\tau)} \leftarrow \mathbf{V}_{\text{cand}}^{(\tau)}$ (Accept momentum step)
 - 22: **else**
 - 23: $\mathbf{U}_{u,n}^{(\tau-1)} \leftarrow \mathbf{V}_{u,n}^{(\tau-1)}$ (Safety Check Failed: Restart)
 - 24: Re-extract $\mathbf{s}_{u,i}^{(\tau)}$, re-predict $\alpha_{u,i}^{(\tau)}$, and update $\mathbf{V}_{u,n}^{(\tau)}$.
 - 25: **end if**
 - 26: **until** objective converges or $\tau = T_{\text{inf}}$
 - 27: **output:** Final beamforming matrices \mathbf{V}
-

heuristic matching weights $\xi_{u,i,n}^{(\tau)}$ or directly predicting discrete assignments, K-Net exclusively determines the *priority order* in which logical transmission slots select RBGs. Each slot then greedily selects its optimal RBG based on the original FastFP metric. This ordering-based design retains the physical interpretability of the assignment weights and significantly reduces the allocation complexity from $\mathcal{O}(UK^3)$ (for per-user Hungarian matching) to $\mathcal{O}(UK^2)$ (for sequential greedy allocation).

1) *Markov Decision Process (MDP) Formulation:* We cast the long-horizon RBG scheduling task as a finite-horizon MDP embedded within the alternating optimization loop. To optimize the full trajectory under a finite iteration budget T , the macro-components of the MDP are formally structured as follows:

- **State** ($s^{(\tau)}$): The state space aggregates the underlying multi-cell topology and algorithmic states, which will be detailed later.
- **Action** ($a^{(\tau)}$): Rather than directly predicting the binary assignment matrix, the action space is defined as the priority scheduling order for all users, denoted as $a^{(\tau)} = \{\pi_u^{(\tau)}\}_{u=1}^U$, where each $\pi_u^{(\tau)}$ is a structural permutation of the logical slots $[N]$.
- **Transition** (\mathcal{T}): The environment state evolves deterministically via a transition function $\mathcal{T} : \mathcal{S} \times \mathcal{A} \rightarrow \mathcal{S}$,

expressed as $s^{(\tau+1)} = \mathcal{T}(s^{(\tau)}, a^{(\tau)})$. Specifically, the action $a^{(\tau)}$ is first mapped by the priority-greedy decoder to reconstruct the discrete allocation $\mathbf{k}^{(\tau)}$, which subsequently triggers the model-driven continuous updates to yield the next optimization state.

- **Reward (R_b):** To enforce trajectory-optimal behavior, an episodic terminal reward is evaluated for the b -th sample at the terminal horizon T , defined as the utility gain over the myopic Hungarian baseline:

$$R_b = F\left(\mathbf{V}_{\theta,b}^{(T)}, \mathbf{k}_{\theta,b}^{(T)}\right) - F\left(\mathbf{V}_{\text{ref},b}^{(T)}, \mathbf{k}_{\text{ref},b}^{(T)}\right), \quad (35)$$

where $F(\cdot)$ denotes the terminal network weighted sum-rate (WSR).

- **Discount Factor (γ):** A parameter $\gamma \in [0, 1]$ that dictates the importance of long-term trajectory gains over immediate improvements.

For the state feature, we construct a compact six-dimensional vector $\mathbf{e}_{u,i,n}^{(\tau)}$ for each candidate edge (u, i, n) :

$$\mathbf{e}_{u,i,n}^{(\tau)} = [e_1, e_2, e_3, e_4, e_5, e_6]. \quad (36)$$

To ensure training stability, all continuous scalar features are normalized via sample-wise standardization with logarithmic pre-scaling. The elements of the state feature vector are defined as:

- **Edge Weight (e_1):** A global representation integrates the analytical matching weight $\xi_{u,i,n}^{(\tau)}$, the signal gain component, and the interference penalty in (21).
- **Allocation and Activation Status (e_2):** A status indicator comprising the binary allocation variable $x_{u,i,n}^{(\tau-1)} \in \{0, 1\}$ and the logical slot activation flag $a_{u,i}^{(\tau-1)} = \sum_{n \in [K]} x_{u,i,n}^{(\tau-1)} \in \{0, 1\}$.
- **Candidate Power Occupation (e_3):** The normalized power consumption of the candidate beamformer, expressed as $p_{u,i,n}^{(\tau)} = \|\widehat{\mathbf{V}}_{u,i,n}^{(\tau)}\|_F^2 / (P_{\max})$, characterizing the proximity to the continuous constraint boundary.
- **Effective Achievable Rate (e_4):** The effective data rate supported at the current slot, evaluated by the term $\rho_{u,i}^{(\tau)} = \frac{1}{d_u} \log \det(\mathbf{I}_{d_u} + \mathbf{\Gamma}_{u,i}^{(\tau)})$.
- **Interference Penalty Weight (e_5):** The receiver-side weighting term that scales the penalty for co-channel interference in the FP objective, defined via the decoding trace $\chi_{u,i}^{(\tau)} = \frac{1}{M_r d_u} \text{Tr}(\mathbf{Y}_{u,i}^{(\tau)}(\mathbf{I}_{d_u} + \mathbf{\Gamma}_{u,i}^{(\tau)})\mathbf{Y}_{u,i}^{(\tau)H})$.
- **Temporal Progress (e_6):** An iteration-aging parameter given by $\eta_\tau = \frac{\tau}{\tau + c_K}$, allowing the recurrent policy to adaptively switch behaviors between early-stage exploration and late-stage fine-tuning.

2) **Global-Pooling Priority Network:** K-Net maps the raw edge feature tensor $\mathbf{E}^{(\tau)} = \{\mathbf{e}_{u,i,n}^{(\tau)}\}$ to scalar slot-priority logits through a series of shared edge embeddings and multi-scale pooling operations. First, each candidate edge is mapped into a high-dimensional representation via a shared NN denoted by ψ_e , which is given by

$$\mathbf{h}_{u,i,n}^0 = \psi_e\left(\mathbf{e}_{u,i,n}^{(\tau)}\right) \in \mathbb{R}^{d_h}. \quad (37)$$

To capture the complex multi-user interference topology, K-Net subsequently aggregates hierarchical context vectors—specifically at the slot, user, RBG, base station (BS), and global network levels. These contextual representations are respectively formulated as

$$\mathbf{c}_{u,i}^S = \psi_S\left(\frac{1}{K} \sum_{n \in [K]} \mathbf{h}_{u,i,n}^0\right), \quad (38a)$$

$$\mathbf{c}_u^U = \psi_U\left(\frac{1}{NK} \sum_{i \in [N]} \sum_{n \in [K]} \mathbf{h}_{u,i,n}^0\right), \quad (38b)$$

$$\mathbf{c}_n^R = \psi_R\left(\frac{1}{UN} \sum_{u \in [U]} \sum_{i \in [N]} \mathbf{h}_{u,i,n}^0\right), \quad (38c)$$

$$\mathbf{c}_b^B = \psi_B\left(\frac{1}{|\mathcal{U}_b|NK} \sum_{u \in \mathcal{U}_b} \sum_{i \in [N]} \sum_{n \in [K]} \mathbf{h}_{u,i,n}^0\right), \quad (38d)$$

$$\mathbf{c}^G = \psi_G\left(\frac{1}{UNK} \sum_{u \in [U]} \sum_{i \in [N]} \sum_{n \in [K]} \mathbf{h}_{u,i,n}^0\right), \quad (38e)$$

where ψ_S , ψ_U , ψ_R , ψ_B , and ψ_G denote dedicated NNs designed to extract distinct levels of topological features. These pooled representations effectively equip K-Net with comprehensive information regarding local candidate qualities, per-slot competition intensity, per-user allocation status, RBG congestion, cell-level load, and the global network environment. By integrating these hierarchical contexts, the fused edge representation is computed via a fusion network ψ_F , expressed as

$$\mathbf{z}_{u,i,n} = \psi_F\left(\mathbf{h}_{u,i,n}^0 + \mathbf{c}_{u,i}^S + \mathbf{c}_u^U + \mathbf{c}_n^R + \mathbf{c}_{b_u}^B + \mathbf{c}^G\right). \quad (39)$$

Subsequently, the slot-level representation is derived by performing an average pooling over all RBG candidates, given by

$$\mathbf{z}_{u,i}^S = \frac{1}{K} \sum_{n \in [K]} \mathbf{z}_{u,i,n}, \quad (40)$$

which is ultimately mapped to a scalar priority logit via a linear output layer ψ_{out} , yielding

$$o_{u,i}^{(\tau)} = \psi_{out}(\mathbf{z}_{u,i}^S). \quad (41)$$

Remarkably, since all constituent NNs are shared across users, slots, RBGs, BSs, and unfolding iterations, the total number of trainable parameters remains strictly independent of the system dimensions (U , N , and K). Consequently, the forward inference computation scales efficiently and linearly with the number of candidate edges.

3) **Priority-Greedy RBG Decoding:** During the stochastic training phase, the discrete slot priority order $\pi_u^{(\tau)}$ is sampled from a Plackett–Luce distribution parameterized by the predicted logits. For each user u , the probability of realizing a specific permutation is defined as

$$p_\theta\left(\pi_u^{(\tau)} \mid s^{(\tau)}\right) = \prod_{\ell=1}^N \frac{\exp\left(o_{u,\pi_{u,\ell}}^{(\tau)} / T_K\right)}{\sum_{j \in \mathcal{J}_{u,\ell}} \exp\left(o_{u,j}^{(\tau)} / T_K\right)}, \quad (42)$$

where T_K is the sampling temperature controlling the exploration variance, and $\mathcal{J}_{u,\ell}$ denotes the set of remaining unselected slots prior to the ℓ -th decoding step. Assuming conditionally independent decisions across users, the joint network policy factorizes as

$$p_\theta \left(a^{(\tau)} \mid s^{(\tau)} \right) = \prod_{u=1}^U p_\theta \left(\pi_u^{(\tau)} \mid s^{(\tau)} \right). \quad (43)$$

Conversely, during the deterministic inference phase, the slots are simply sorted in descending order based on the logits $o_{u,i}^{(\tau)}$ to form the exact priority sequence.

Given the priority sequence $\pi_u^{(\tau)}$, K-Net employs a sequential greedy decoding scheme. Let $\mathcal{R}_{u,\ell}$ denote the subset of physical RBGs that remain available to user u before decoding the ℓ -th slot. The optimally selected RBG $n_{u,\ell}^*$ for the current slot is determined by greedily maximizing the analytical matching weight:

$$n_{u,\ell}^* = \arg \max_{n \in \mathcal{R}_{u,\ell}} \xi_{u,\pi_u,\ell,n}^{(\tau)}. \quad (44)$$

Accordingly, the exact binary decision is formalized as

$$x_{u,\pi_u,\ell,n}^{(\tau)} = \begin{cases} 1, & \text{if } n = n_{u,\ell}^* \text{ and } \xi_{u,\pi_u,\ell,n_{u,\ell}^*}^{(\tau)} > 0, \\ 0, & \text{otherwise.} \end{cases} \quad (45)$$

As explicitly constrained by (45), if the maximum available matching weight is nonpositive, the corresponding slot remains inactive to prevent WSR degradation. Crucially, this decoding paradigm retains the physics-informed matching weight $\xi_{u,i,n}^{(\tau)}$, while exclusively optimizing the sequential order in which slots compete for resources. Furthermore, when assuming $N = K$, this decoding paradigm has complexity $\mathcal{O}(UK^2)$ smaller than $\mathcal{O}(UK^3)$ for per-user Hungarian matching.

4) *Policy-Gradient Training*: The training objective of K-Net is to maximize the expected terminal WSR:

$$\mathcal{J}(\theta) = \mathbb{E}_{p_\theta} \left[F \left(\mathbf{V}^{(T)}, \mathbf{k}^{(T)} \right) \right]. \quad (46)$$

To directly optimize this objective over the discrete action space, we employ the REINFORCE policy-gradient estimator [37]. The corresponding policy gradient is formulated as:

$$\nabla_\theta \mathcal{J}(\theta) = \mathbb{E}_{p_\theta} \left[R_b \sum_{\tau=1}^T \nabla_\theta \log p_\theta \left(a^{(\tau)} \mid s^{(\tau)} \right) \right]. \quad (47)$$

To effectively reduce the variance of the gradient estimation, the advantage term R_b is explicitly designed as the terminal utility gain over the traditional deterministic optimization algorithm in section III.

The proposed K-Net leverages the analytical FastFP edge weighting as a physics-informed utility, while learning an ordering policy that optimizes the long-term allocation trajectory. Consequently, K-Net significantly improves the terminal WSR under a strict unfolding budget, preserving the low-complexity advantage of sequential greedy allocation.

V. NUMERICAL RESULTS

In this section, we evaluate the proposed deep-unfolding framework through extensive numerical simulations. First, we outline the simulation setup. Next, to explicitly isolate the contribution of the continuous beamforming optimizer, we evaluate P-Net under fixed RBG assignments. In this part, we analyze its WSR acceleration capability, convergence behavior, the distribution of the learned relaxation factor α , and its robustness across unseen network scales and channel conditions. Finally, we evaluate the complete joint resource allocation and beamforming framework. Within this joint setting, we first demonstrate how the policy-guided K-Net mitigates the performance degradation introduced by low-complexity greedy scheduling with well-learned decoding order, and then showcase how the combined P-Net and K-Net architecture achieves a superior complexity-performance trade-off compared to conventional model-driven joint optimization baselines.

A. Simulation Setup

We consider a multi-cell downlink MIMO network with a hexagonal cell layout, where each BS is located at the center of a cell, and users are uniformly distributed within the service area. All BSs share the same set of RBGs, and the distance between adjacent BSs is set to $D = 0.8$ km. The number of data streams is identical for all users and satisfies $d_u = 2$. Each BS is equipped with $M_t = 32$ transmit antennas, and each user is equipped with $M_r = 4$ receive antennas. The maximum transmit power is $P_{\max} = 40$ dBm. The noise power density is set to $N_0 = -174$ dBm/Hz, and the bandwidth is set to 180 kHz. The distance-dependent path-loss model follows: $PL(r) = 128.1 + 37.6 \log_{10}(r) + \xi$, where r is the transmission distance in kilometers and $\xi \sim \mathcal{N}(0, 8^2)$ models log-normal shadowing. All user weights are identical and set to $\rho_u = 1$. Independent channel realizations are generated and divided into training and test sets. The initial RBG assignment is constructed based on the direct channel gain, and the initial beamformer is initiated randomly, followed by power projection.

The P-Net is implemented as a recurrent optimizer based on a single-layer GRU with 128 hidden units. The input features are normalized before being fed into the network. The GRU parameters are shared across all unfolded optimization iterations, allowing the trained model to be evaluated with an inference horizon different from the training horizon. For the TBPTT training, we roll out the recurrent optimizer for $T = 100$ optimization iterations and apply truncated backpropagation through time with a truncation length of $l = 10$. Therefore, the rollout is partitioned into 10 consecutive chunks. For K-Net, all NN modules—including the shared edge embedding, multi-scale context encoders, and the feature fusion layer—are implemented as two-layer MLPs with 32 hidden units. In addition, both P-Net and K-Net are optimized using the Adam optimizer.

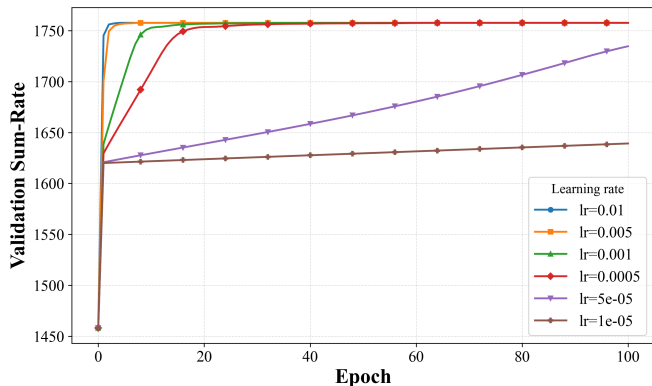


Fig. 4. Validation weighted sum-rate (WSR) trajectories of P-Net under different learning rates during the training phase.

B. Performance Evaluation under Fixed RBG Allocation

To strictly isolate the contribution of the continuous beamforming optimizer, we first evaluate P-Net under fixed RBG assignments. In this specific setting, to ensure a fair comparison with the standard FP benchmarks [33], we temporarily replace the per-beamformer power constraint defined in (4b) with a base-station (BS)-level sum-power constraint: $\sum_{u \in \mathcal{U}_b} \sum_{i \in [N]} \text{Tr}(\mathbf{V}_{u,i} \mathbf{V}_{u,i}^H) \leq P_{\max}, \forall b \in \mathcal{A}$. Consequently, the continuous FastFP update rules must be adapted to accommodate this BS-level constraint. Specifically, the scalar curvature bound λ in the gradient step must be unified across all active links within the same cell, defined as $\lambda_b = \max_{u \in \mathcal{U}_b, i \in [N]} \lambda_{\max}(\mathbf{L}_{u,i})$. The corresponding unconstrained update and the BS-level power projection are respectively modified as:

$$\tilde{\mathbf{V}}_{u,i}^{(\tau)} = \mathbf{V}_{u,i}^{(\tau-1)} + \frac{1}{\lambda_{b_u}} \left(\mathbf{A}_{u,i} - \mathbf{L}_{u,i} \mathbf{V}_{u,i}^{(\tau-1)} \right)$$

and

$$\mathbf{V}_{u,n}^{(\tau)} = \begin{cases} \tilde{\mathbf{V}}_{u,n}^{(\tau)}, & \text{if } S_b \leq P_{\max}, \\ \sqrt{\frac{P_{\max}}{S_b}} \tilde{\mathbf{V}}_{u,n}^{(\tau)}, & \text{otherwise,} \end{cases}$$

where $S_b = \sum_{u \in \mathcal{U}_b} \sum_i \text{Tr}(\tilde{\mathbf{V}}_{u,i}^{(\tau)} \tilde{\mathbf{V}}_{u,i}^{(\tau)H})$ denotes the total unconstrained transmit power of BS b . Unless otherwise specified, the surrogate safety-check procedure is disabled during inference, as it is rarely activated in practice. Therefore, the results mainly reflect the intrinsic acceleration behavior of P-Net.

1) *Training Dynamics*: We first examine the training behavior of P-Net and the effect of key hyperparameters in the setting with $B = 7$ BSs, $U = 14$ users, and $K = 14$ RBGs. Fig. 4 and Fig. 5 illustrate the validation WSR trajectories under varying learning rates and batch sizes, respectively. A learning rate of 10^{-3} and a moderate batch size of 16 are empirically selected to balance convergence speed and training stability. The smooth saturation of these validation curves confirms that the proposed recurrent parameter-sharing structure can be reliably optimized across unfolded iterations.

2) *WSR Performance and Acceleration Ability*: We then evaluate the beamforming performance of P-Net against representative iterative baselines. The compared methods are summarized as follows.

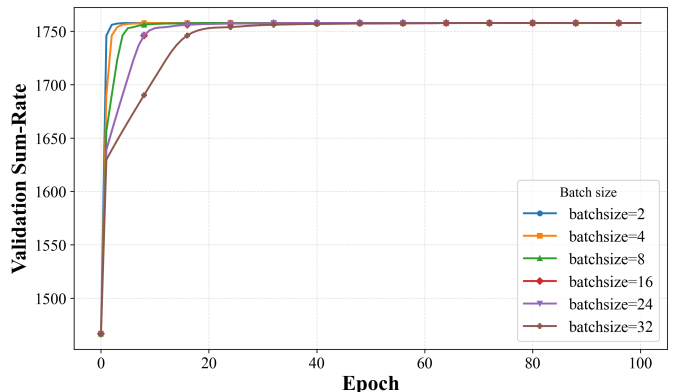


Fig. 5. Validation weighted sum-rate (WSR) trajectories of P-Net under different batch sizes.

- **FastFP**: The state-of-the-art (SOTA) inversion-free FP benchmark based on the nonhomogeneous bound [33] whose optimization trajectory can be conservative due to the worst-case spectral radius step size.
- **Nesterov-FastFP**: A momentum-accelerated variant of FastFP that integrates Nesterov's extrapolation strategy to expedite the model-driven continuous optimization trajectory.
- **DeepFP-hybrid [31]**: A latest deep-unfolded FP baseline that unrolls a fixed number of FastFP iterations into neural network layers. In each layer, the analytical updates of the FP auxiliary variables and beamformers are preserved, while a DNN predicts the user-wise stepsize $\lambda^{(\tau)}$. The network is first pre-trained by supervised distillation using beamforming labels generated by 100-iteration Nesterov-FastFP, and is then fine-tuned by maximizing the WSR objective.
- **DeepFP-unsupervised [31]**: An unsupervised counterpart of DeepFP-hybrid with the same fixed-depth unfolded FastFP architecture. Instead of using labels, it is trained from scratch by minimizing the negative WSR evaluated at the terminal unfolded layer.

We first consider the scenario setting with $B = 7$, $U = 28$, and $K = 14$. All algorithms are evaluated over 1000 independent channel realizations sampled from the same environment setting. Fig. 6 shows the corresponding cumulative distribution function (CDF). Compared with FastFP and Nesterov-FastFP, the distribution of P-Net is shifted toward the high-WSR region, indicating that the gain is not limited to the average value; P-Net also improves lower-percentile and median performance on the test samples. The acceleration effect is further quantified in Table I. We use the WSR achieved by Nesterov-FastFP after 100 iterations as the reference target. P-Net reaches this target within 55 iterations and requires 116.74 milliseconds, whereas the 100-iteration Nesterov-FastFP reference requires 194.34 milliseconds. Although the per-iteration runtime of P-Net is slightly higher due to neural network inference, the reduced number of iterations results in lower total inference time. FastFP does not reach the same target within 100 iterations under this setting.

We further benchmark it against learning-based methods

TABLE I
ITERATIONS AND RUNTIME REQUIRED TO MATCH THE 100-ITERATION NESTEROV-FASTFP REFERENCE ($B = 7, U = 28, K = 14$)

Method	WSR at 100 Iter.	Iter. to Target	Time to Target (ms)	Time/Iter. (ms)
Nesterov-FastFP	3485.64	100	194.34 (100%)	1.94
P-Net	3908.35	55	116.74 (60.7%)	2.12
FastFP	2130.00	> 100	–	1.92

TABLE II
COMPARISON WITH FIXED-DEPTH DEEPFP BASELINES UNDER FIXED RBG ASSIGNMENT ($B = 7, U = 28, K = 14$)

Method	Training Signal	Inference Horizon	Avg. WSR	CPU Time (ms)
FastFP	–	100 iter.	2129.72	185.34
Nesterov-FastFP	–	100 iter.	3485.20	180.66
DeepFP-Unsupervised	WSR	8 layers/iter.	1600.85	20.91
DeepFP-Hybrid	Label(100iter.) + WSR	8 layers/iter.	2179.13	17.20
P-Net	WSR	8 iter.	1554.02	16.49
P-Net	WSR	100 iter.	3908.35	185.95

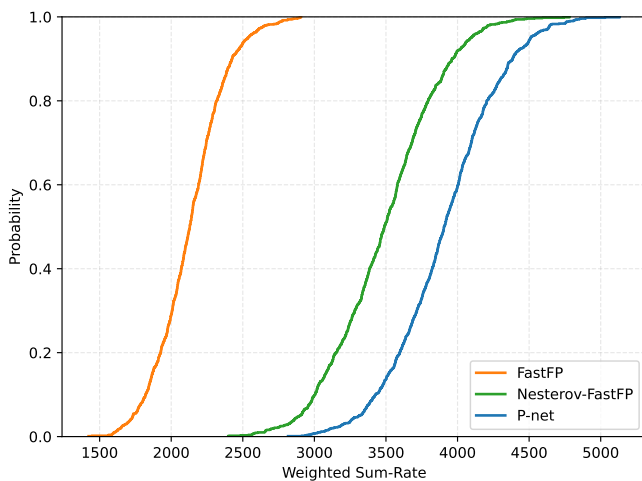


Fig. 6. Cumulative Distribution Function (CDF) of the final WSR for the $B = 7, U = 28,$ and $K = 14$ setting.

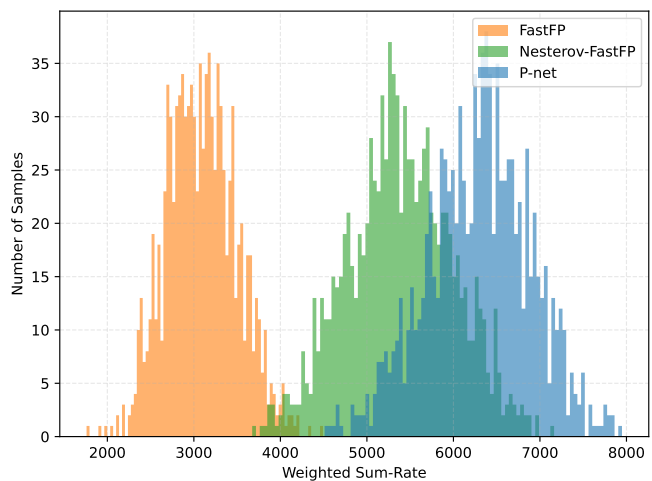


Fig. 7. Weighted Sum-rate distribution in the $B = 7, U = 35,$ and $K = 20$ setting.

to evaluate the structural impact of our recurrent parameter-sharing architecture relative to a fixed-depth unfolding of DeepFP. For both DeepFP baselines, we fix the unfolded depth to $T = 8$ layers. This configuration is primarily chosen to maintain a comparable number of model parameters with P-Net. Table II compares these methods under the same $B = 7, U = 28,$ and $K = 14$ test setting. As observed, DeepFP-Hybrid exhibits a strong short-horizon WSR (2179.13) due to its end-to-end knowledge distillation from a 100-iteration teacher. However, its fixed-depth architecture severely restricts further iterative refinement. In contrast, P-Net functions as a bounded step-size controller; its recurrent parameter-sharing mechanism completely decouples the inference horizon from the training depth. When unfolded to 100 iterations, P-Net achieves an ultimate WSR of 3908.35, outperforming the 100-iteration Nesterov-FastFP reference by 12.1% under a comparable runtime.

We next evaluate a denser setting with $B = 7$ BSs, $U = 35$ users, and $K = 20$ RBGs. The distribution-level results for

the same setting are shown in Fig. 7, which shows that P-Net yields a higher WSR distribution than the considered baselines at the same iteration budget. Hence, the gain observed in the convergence curve is also reflected across the sample-wise performance distribution. To further evaluate the convergence behavior of the P-net, Fig. 8 compares the average WSR trajectories over more than 100 iterations. Enabled by the bounded relaxation factor, P-Net consistently maintains a steeper ascent and achieves a faster convergence rate than both FastFP and Nesterov-FastFP across the entire iteration horizon. To better understand P-Net’s acceleration mechanism, Fig. 9 visualizes the empirical statistics of the learned relaxation factor $\alpha_{u,i}^{(\tau)}$ over these 500 iterations. Structurally bounded within the safe interval $(0, 2)$ to preserve monotonicity, the mean and median of α consistently exceed the standard FastFP baseline ($\alpha = 1$), enabling more aggressive optimization steps. Furthermore, the network learns an iteration-dependent policy: it favors larger relaxation factors during early iterations to expedite progress, and adaptively reduces α in later stages to prevent unstable

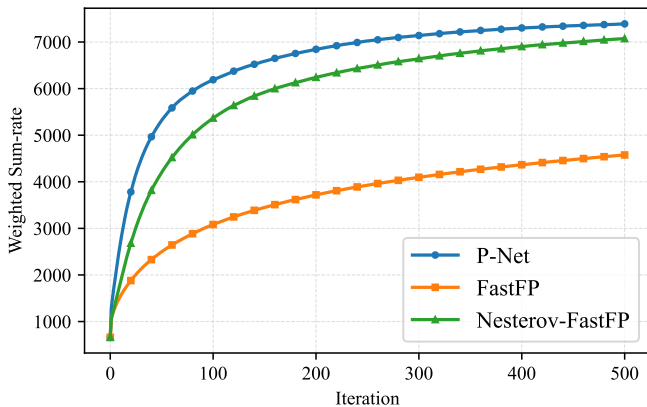


Fig. 8. Average WSR convergence trajectories over 500 iterations in the $B = 7$, $U = 35$, and $K = 20$ setting.

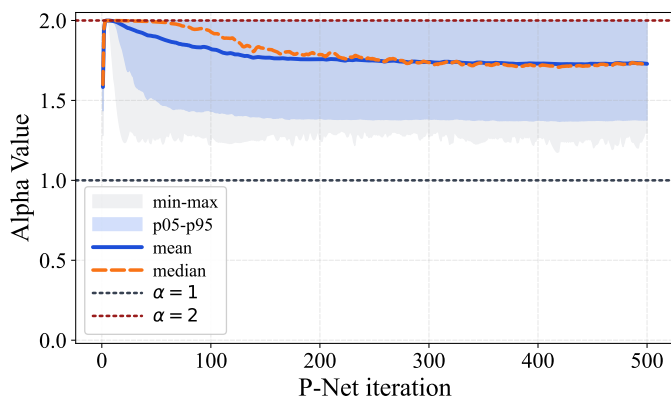


Fig. 9. Statistical distribution (mean, median, and percentiles) of the learned relaxation factor α over 500 optimization iterations in the $B = 7$, $U = 35$, and $K = 20$ setting.

oscillations. This interpretable dynamic confirms that P-Net functions as an adaptive step-size controller rather than a purely black-box beamformer predictor.

3) *Generalization Under Network-Scale Variations*: Since P-Net operates on the physics features of the FastFP framework and shares parameters across user-RB links, it is expected to generalize more naturally across different values of U and K than a fully fixed-dimensional NN. We evaluate this property by training P-Net in the network with $B = 7$ BSs, $U = 28$ users, and $K = 14$ RBGs, and then testing it under network settings with different numbers of users and/or RBGs.

Figs. 10a–10c report the CDFs when the number of RBGs is varied while the number of users remains fixed at $U = 28$. Across different values of K , the P-Net curve consistently shifts to the right of the FastFP and Nesterov-FastFP baselines, indicating that the learned relaxation rule remains effective when the dimension of the RBG set differs from the training setting. Figs. 10d–10f further evaluate the generalization to different numbers of users. These results suggest that P-Net learns a transferable update policy from local optimization-state features, rather than memorizing a fixed network setting policy.

We further evaluate the robustness of P-Net to shifts in

transmit power and shadowing variance. The P-Net model is trained only under the default simulation setting with BS total transmit power $P_{\max} = 40$ dBm and shadowing $\xi \sim \mathcal{N}(0, 8^2)$. The results in Table III show that P-Net outperforms Nesterov-FastFP under all tested transmit power and shadowing variances. Meanwhile, the relative gain becomes smaller as the transmit power decreases. This is because lower transmit power leads to a lower-SNR regime, where both methods are closer to their converged performance after 100 iterations, leaving less room for P-Net to further improve over the baseline. As a result, P-Net achieves modest gains at transmit power of 20 dBm, while its advantage becomes more pronounced in higher-SNR scenarios.

C. Performance Evaluation Under Joint Optimization of RBG Allocation and Beamforming

The preceding experiments under fixed RBG assignments verify that P-Net can accelerate the continuous FastFP beamforming update. We now evaluate the complete joint RBG allocation and beamforming process, where the continuous beamforming step and the discrete RBG scheduling step are updated alternately. This setting is more challenging because the RBG assignment affects the interference topology, while the beamforming update in turn changes the utility of future RBG assignments.

We consider two network scenarios to evaluate whether the proposed modules provide a consistent performance-runtime advantage under different scheduling loads. The first scenario is configured as $B = 7$, $U = 14$, and $K = 28$, where the number of RBGs is relatively abundant compared with the number of users. The second scenario is configured as $B = 7$, $U = 28$, and $K = 35$, where the number of users is doubled and the discrete scheduling competition becomes stronger. For all compared methods, the same channel realizations, initial RBG assignments, and initial beamformers are used in each scenario.

We compare the following four joint optimization methods:

- **FastFP + Hungarian**: the conventional model-driven joint baseline, where the beamforming step uses FastFP and the RBG allocation step is solved by Hungarian matching.
- **FastFP + Greedy**: a low-complexity baseline that uses the priority-greedy RBG decoding process, but follows a fixed default index order of the decision slots.
- **FastFP + K-Net**: an allocation-side learned accelerator, where the beamforming step remains FastFP while K-Net predicts the priority order used by the same greedy RBG decoder.
- **P-Net + K-Net**: the proposed learned joint method, where P-Net accelerates the continuous FastFP beamforming update and K-Net accelerates the discrete RBG allocation step.

This comparison separates the roles of the two learning modules. The gap between FastFP + Greedy and FastFP + K-Net isolates the benefit of learning the priority order for greedy RBG decoding. The gap between FastFP + K-Net and P-Net + K-Net further shows whether P-Net can still provide additional

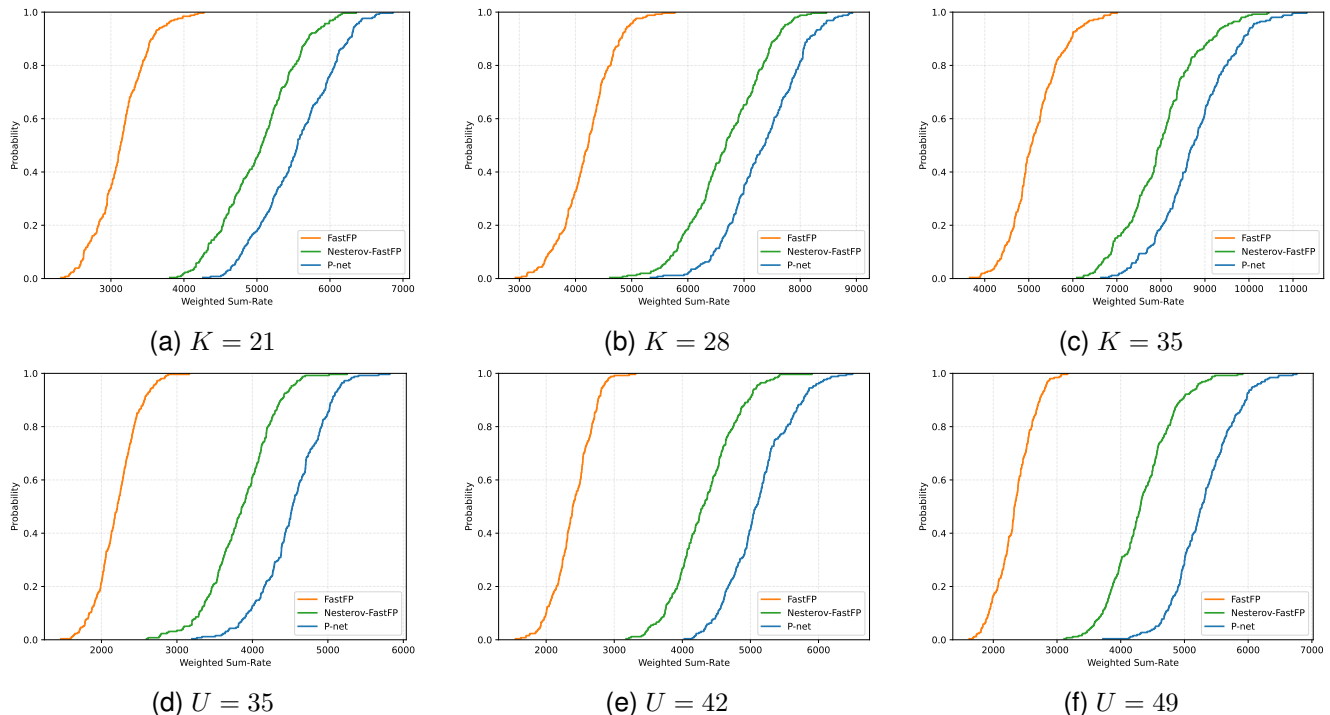


Fig. 10. CDFs of WSR under different system dimensions. The first row evaluates the generalization of P-Net to different numbers of RBGs, while the second row evaluates the generalization to different numbers of users.

TABLE III
P-NET GENERALIZATION UNDER DIFFERENT SHADOWING VARIANCES AND TRANSMIT-POWER BUDGETS WITHOUT RETRAINING

P_{\max} (dBm)	σ_{sh} (dB)	Average WSR After 100 Iterations		Relative Gain	CPU Time (ms)
		P-Net	Nesterov-FastFP		
20	4	1255.77	1248.87	0.55%	126.25 (67.1%)
	8	1476.40	1455.24	1.45%	120.78 (62.1%)
	12	1728.50	1670.63	3.46%	113.75 (59.9%)
30	4	2634.54	2555.88	3.08%	120.93 (62.7%)
	8	2759.19	2628.52	4.97%	133.44 (68.2%)
	12	2826.90	2601.36	8.67%	131.41 (61.8%)
40	4	4126.52	3757.74	9.81%	107.81 (53.0%)
	8	3951.97	3500.98	12.88%	108.29 (57.0%)
	12	3645.41	3090.35	17.96%	111.09 (56.8%)

beamforming acceleration after the discrete allocation step has already been accelerated by K-Net.

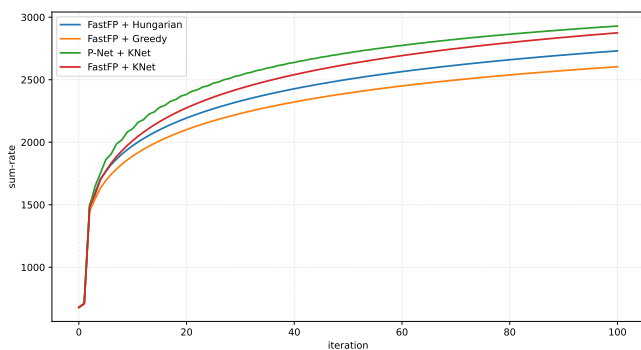
Table IV reports the final WSR and measured runtime per sample of the four joint optimization methods. In Scenario I, FastFP + Greedy reduces the runtime to 31.86% of FastFP + Hungarian, but its final WSR decreases by 4.65%. This confirms that simply replacing Hungarian matching with a fixed-order greedy decoder provides acceleration at a clear performance cost. In contrast, FastFP + K-Net uses the same greedy decoder but replaces the default order with a learned priority order. It improves the final WSR by 5.28% over FastFP + Hungarian while using only 36.74% of the baseline runtime. Therefore, the gain of K-Net comes from learning a better decoding order rather than from changing the underlying FP-derived edge utility or invoking a more expensive assignment solver.

The same conclusion also holds in Scenario II. When the number of users increases from 14 to 28, FastFP + Greedy still remains below FastFP + Hungarian in final WSR. FastFP + K-Net, however, slightly exceeds the Hungarian baseline by 1.13% while reducing the runtime to 50.83%. This result is important because the larger scenario increases the size and difficulty of the discrete scheduling problem, yet K-Net still preserves the WSR quality of Hungarian matching with much lower inference time.

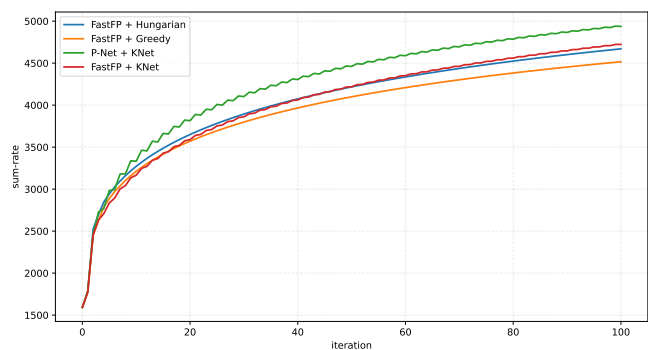
The complete P-Net + K-Net method further strengthens this advantage in both scenarios. In Scenario I, it improves the WSR gain from 5.28% to 7.27% over FastFP + Hungarian and reaches the final Hungarian target using only 19.46% of the baseline time. In Scenario II, the additional contribution of P-Net becomes more pronounced: P-Net + K-Net improves the final WSR by 5.71% over FastFP + Hungarian and by

TABLE IV
PERFORMANCE AND RUNTIME SUMMARY FOR JOINT RBG ALLOCATION AND BEAMFORMING

Scenario	Method	Final WSR	WSR Gain	CPU time (s)	Time Ratio	Speedup	Target Iter./Time
7BS-14UE-28RB	FastFP + Hungarian	2730.70	Ref.	4.60	100.00%	1.00×	100/4.60 (100.00%)
	FastFP + Greedy	2603.77	-4.65%	1.47	31.86%	3.14×	-
	FastFP + K-Net	2874.88	+5.28%	1.69	36.74%	2.72×	67/1.13 (24.62%)
	P-Net + K-Net	2929.13	+7.27%	1.69	36.72%	2.72×	53/0.89 (19.46%)
7BS-28UE-35RB	FastFP + Hungarian	4670.34	Ref.	8.91	100.00%	1.00×	100/8.91 (100.00%)
	FastFP + Greedy	4516.82	-3.29%	4.32	48.46%	2.06×	-
	FastFP + K-Net	4722.97	+1.13%	4.53	50.83%	1.97×	93/4.21 (47.27%)
	P-Net + K-Net	4936.90	+5.71%	4.55	51.02%	1.96×	67/3.05 (34.18%)



(a) $B = 7, U = 14, K = 28$.



(b) $B = 7, U = 28, K = 35$.

Fig. 11. Average WSR trajectories of joint RBG allocation and beamforming optimization.

4.53% over FastFP + K-Net. These results show that K-Net addresses the discrete-matching bottleneck, while P-Net further accelerates and improves the continuous beamforming trajectory after the allocation step has been changed.

Fig. 11 compares the WSR trajectories of the four methods. In both scenarios, FastFP + Greedy remains below FastFP + Hungarian, indicating that the fixed default priority order is insufficient to preserve the performance of joint optimization. FastFP + K-Net reaches or exceeds the final FastFP + Hungarian target with substantially fewer effective runtimes. Specifically, it reaches the target at the 67-th iteration in Scenario I and at the 93-rd iteration in Scenario II. P-Net + K-Net reaches the same target earlier, at the 53-rd and 67-th iterations, respectively. This demonstrates that the learned continuous and discrete modules are complementary: K-Net avoids the high cost of Hungarian matching, while P-Net further shortens the trajectory required to reach the same WSR level. It is also observed that the K-Net-based trajectories may exhibit mild non-monotonic fluctuations. This behavior is expected in joint RBG allocation and beamforming. Because K-Net is trained to improve the long-horizon terminal WSR rather than enforce monotonic improvement at every discrete reassignment step.

Fig. 12 reports the sample-wise final WSR distributions. The CDFs show that FastFP + K-Net and P-Net + K-Net shift the WSR distribution to the right of FastFP + Hungarian in both scenarios. Hence, the average WSR gain is not caused by

a few favorable channel realizations, but appears consistently across the test distribution. Among all methods, P-Net + K-Net produces the most favorable distribution, confirming that the learned continuous beamforming acceleration and learned discrete priority scheduling jointly improve the performance-runtime tradeoff.

VI. CONCLUSION

In this paper, we proposed a joint deep unfolding framework, comprising P-Net and K-Net, to tackle the mixed-integer RBG scheduling and beamforming problem in multi-cell MIMO networks. For continuous beamforming, P-Net accelerates the FastFP trajectory by learning a bounded relaxation factor, ensuring rapid convergence while strictly preserving theoretical monotonic ascent and stationary-point guarantees. For discrete scheduling, K-Net learns a priority policy that guides a low-complexity greedy allocation, effectively bypassing the prohibitive overhead of Hungarian matching without sacrificing assignment quality. By leveraging recurrent parameter sharing, both networks achieve a minimal memory footprint and support flexible inference beyond the training horizon. Extensive simulations confirm that the proposed framework achieves a superior WSR-runtime trade-off compared to conventional model-driven baselines, while generalizing robustly to unseen network scales, antenna configurations, and channel conditions without retraining.

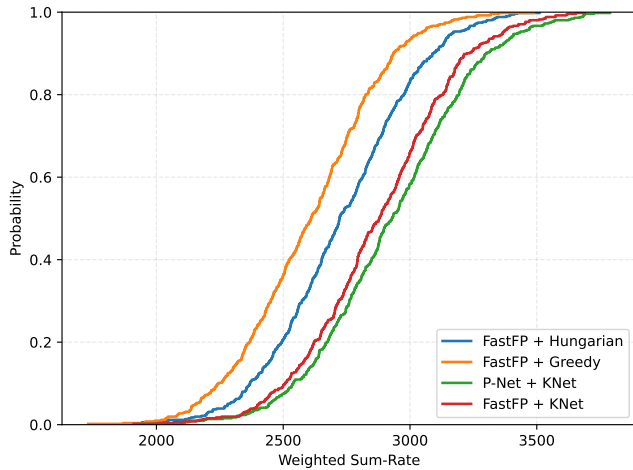
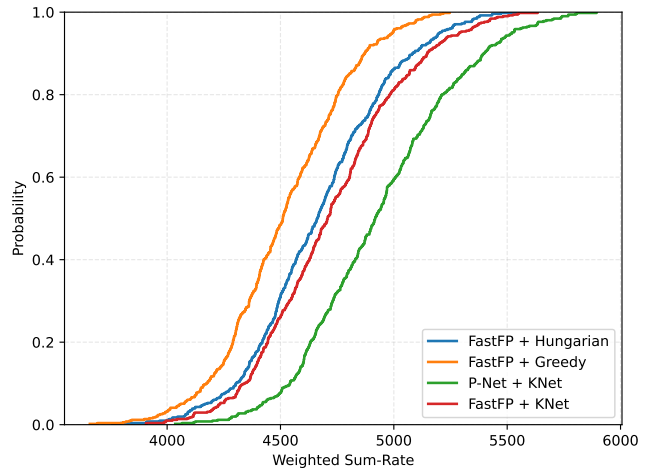
(a) CDF, $B = 7, U = 14, K = 28$.(b) CDF, $B = 7, U = 28, K = 35$.

Fig. 12. Final WSR CDF under joint RBG allocation and beamforming optimization.

APPENDIX A PROOF OF LEMMA 2

In this appendix, we provide the detailed proof of Lemma 2, which mathematically establishes the monotonic non-decreasing property of the proposed P-Net update rule.

Proof. The FastFP algorithm operates within a MM framework [33]. As conceptually illustrated in Fig. 3, at an arbitrary τ iteration, the surrogate function $Q(\mathbf{V} | \mathbf{V}^{(\tau-1)})$ acts as a tight lower bound (minorant) to the true objective $f(\mathbf{V})$, satisfying the global minorization property $Q(\mathbf{V} | \mathbf{V}^{(\tau-1)}) \leq f(\mathbf{V})$ and tight bound at the expansion point $Q(\mathbf{V}^{(\tau-1)} | \mathbf{V}^{(\tau-1)}) = f(\mathbf{V}^{(\tau-1)})$.

By completing the square with respect to \mathbf{V} , the surrogate function $Q(\mathbf{V} | \mathbf{V}^{(\tau-1)})$ can be equivalently rewritten as:

$$Q(\mathbf{V} | \mathbf{V}^{(\tau-1)}) = -\lambda \|\mathbf{V} - \mathbf{V}^{\text{FP}}\|_F^2 + C'$$

where $C' = \frac{1}{\lambda} \|\Xi\|_F^2 + C$ is a term independent of \mathbf{V} , and $\mathbf{V}^{\text{FP}} = \frac{1}{\lambda} \Xi$ is the unconstrained maximizer.

Let $\Delta \mathbf{V} \triangleq \mathbf{V}^{\text{FP}} - \mathbf{V}^{(\tau-1)}$ denote the update direction. The P-Net update rule is formulated as $\mathbf{V}^{(\tau)} = \mathbf{V}^{(\tau-1)} + \alpha \Delta \mathbf{V}$. Substituting this into the surrogate function yields:

$$\begin{aligned} Q(\mathbf{V}^{(\tau)} | \mathbf{V}^{(\tau-1)}) &= -\lambda \|\mathbf{V}^{(\tau-1)} + \alpha \Delta \mathbf{V} - \mathbf{V}^{\text{FP}}\|_F^2 + C' \\ &= -\lambda \|(\alpha - 1) \Delta \mathbf{V}\|_F^2 + C' \\ &= -\lambda (\alpha - 1)^2 \|\Delta \mathbf{V}\|_F^2 + C'. \end{aligned}$$

Similarly, evaluating the surrogate at the expansion point $\mathbf{V}^{(\tau-1)}$ gives $Q(\mathbf{V}^{(\tau-1)} | \mathbf{V}^{(\tau-1)}) = -\lambda \|\Delta \mathbf{V}\|_F^2 + C'$.

The elevation of the surrogate function can be mathematically quantified as:

$$\begin{aligned} Q(\mathbf{V}^{(\tau)} | \mathbf{V}^{(\tau-1)}) - Q(\mathbf{V}^{(\tau-1)} | \mathbf{V}^{(\tau-1)}) & \\ &= \lambda (1 - (\alpha - 1)^2) \|\Delta \mathbf{V}\|_F^2 \\ &= \lambda \alpha (2 - \alpha) \|\Delta \mathbf{V}\|_F^2. \end{aligned}$$

Since $\lambda > 0$ and $\|\Delta \mathbf{V}\|_F^2 \geq 0$, the condition for strict surrogate ascent is $\alpha(2 - \alpha) \geq 0$. The P-Net structurally bounds

the relaxation factor to $\alpha \in (0, 2)$, which strictly satisfies this inequality, thereby guaranteeing $Q(\mathbf{V}^{(\tau)} | \mathbf{V}^{(\tau-1)}) \geq Q(\mathbf{V}^{(\tau-1)} | \mathbf{V}^{(\tau-1)})$.

Combining this with the properties of the MM framework, we deduce:

$$\begin{aligned} f(\mathbf{V}^{(\tau)}) &\geq Q(\mathbf{V}^{(\tau)} | \mathbf{V}^{(\tau-1)}) \\ &\geq Q(\mathbf{V}^{(\tau-1)} | \mathbf{V}^{(\tau-1)}) = f(\mathbf{V}^{(\tau-1)}) \end{aligned}$$

This confirms the monotonic non-decreasing of the objective function. \square

APPENDIX B PROOF OF THEOREM 1

In this appendix, we provide the detailed proof of Theorem 1 about the proposed algorithm converging to a stationary point of the original optimization problem.

Proof. First, given the compact transmit power constraints in (4b) and the finite additive noise, the weighted sum-rate objective function $f(\mathbf{V})$ is upper-bounded. Since Lemma 2 guarantees that the sequence of objective values $\{f(\mathbf{V}^{(\tau)})\}$ is monotonically non-decreasing, it must converge to a finite limit f^* . Furthermore, owing to the compactness of the feasible set \mathcal{W} enforced by the power constraints, the sequence of beamformers $\{\mathbf{V}^{(\tau)}\}$ possesses at least one limit point, denoted by \mathbf{V}^* .

As $\tau \rightarrow \infty$, the parameterized update rule in (28) yields the limiting relation $\mathbf{V}^* = \mathbf{V}^* + \alpha(\mathbf{V}^{\text{FP}*} - \mathbf{V}^*)$, where $\mathbf{V}^{\text{FP}*}$ represents the analytical FastFP guide evaluated at \mathbf{V}^* . Given that the neural network structurally ensures the relaxation factor $\alpha > 0$, this equality holds if and only if $\mathbf{V}^* = \mathbf{V}^{\text{FP}*}$. Since $\mathbf{V}^{\text{FP}*}$ is mathematically equivalent to a gradient projection operation on the local surrogate function Q , the limit point \mathbf{V}^* must satisfy the projected fixed-point condition of the surrogate problem:

$$\mathbf{V}^* = \mathcal{P}_{\mathcal{W}} \left(\mathbf{V}^* + \frac{1}{\lambda} \nabla_{\mathbf{V}} Q(\mathbf{V}^* | \mathbf{V}^*) \right).$$

According to the first-order gradient matching property of the MM framework, the gradient of the true objective function and the surrogate function are identical at the expansion point, i.e., $\nabla_{\mathbf{V}}f(\mathbf{V}^*) = \nabla_{\mathbf{V}}Q(\mathbf{V}^* | \mathbf{V}^*)$. Substituting this into the fixed-point relation yields:

$$\mathbf{V}^* = \mathcal{P}_{\mathcal{W}} \left(\mathbf{V}^* + \frac{1}{\lambda} \nabla_{\mathbf{V}}f(\mathbf{V}^*) \right).$$

This explicitly satisfies the projected gradient stationary condition for the original constrained optimization problem in (4), which concludes the proof that the limit point \mathbf{V}^* is a stationary point of $f(\mathbf{V})$. \square

REFERENCES

- [1] ITU Radiocommunication Sector, "Framework and overall objectives of the future development of imt for 2030 and beyond," International Telecommunication Union, Recommendation ITU-R M.2160-0, November 2023. [Online]. Available: <https://itu.int>
- [2] Ericsson, "Ericsson mobility report june 2024," Ericsson, Tech. Rep., Jun. 2024. [Online]. Available: <https://www.ericsson.com/en/reports-and-papers/mobility-report>
- [3] H. Tataria, M. Shafi, A. F. Molisch, M. Dohler, H. Sjöland, and F. Tufvesson, "6G wireless systems: Vision, requirements, challenges, insights, and opportunities," *Proceedings of the IEEE*, vol. 109, no. 7, pp. 1166–1199, 2021.
- [4] K. B. Letaief, W. Chen, Y. Shi, J. Zhang, and Y.-J. A. Zhang, "The roadmap to 6g: Ai empowered wireless networks," *IEEE communications magazine*, vol. 57, no. 8, pp. 84–90, 2019.
- [5] D. Gesbert, S. Hanly, H. Huang, S. Shamai, O. Simeone, and W. Yu, "Multi-cell MIMO cooperative networks: A new look at interference," *IEEE Journal on Selected Areas in Communications*, vol. 28, no. 9, pp. 1380–1408, 2010.
- [6] E. Björnson and E. Jorswieck, "Optimal resource allocation in coordinated multi-cell systems," *Foundations and Trends in Communications and Information Theory*, vol. 9, no. 2–3, pp. 113–381, 2013.
- [7] J. Huang, V. G. Subramanian, R. Agrawal, and R. A. Berry, "Downlink scheduling and resource allocation for ofdm systems," *IEEE Transactions on Wireless Communications*, vol. 8, no. 1, pp. 288–296, 2009.
- [8] Y.-F. Liu and Y.-H. Dai, "On the complexity of joint subcarrier and power allocation for multi-user ofdma systems," *IEEE Transactions on Signal Processing*, vol. 62, no. 3, pp. 583–596, 2014.
- [9] B. Song, Y.-H. Lin, and R. L. Cruz, "Weighted max-min fair beamforming, power control, and scheduling for a miso downlink," *IEEE Transactions on Wireless Communications*, vol. 7, no. 2, pp. 464–469, 2008.
- [10] W. Yu, T. Kwon, and C. Shin, "Multicell coordination via joint scheduling, beamforming, and power spectrum adaptation," in *Proceedings IEEE INFOCOM*, 2011, pp. 2570–2578.
- [11] N. U. Hassan and M. Assaad, "Downlink beamforming and resource allocation in multicell MISO-OFDMA systems," *Transactions on Emerging Telecommunications Technologies*, vol. 25, no. 2, pp. 173–182, 2014.
- [12] A. Khanafer, T. J. Lim, R. Doostnejad, and T. Tang, "MIMO-OFDMA rate allocation and beamformer design using a multi-access channel framework," in *IEEE International Conference on Communications*, 2012, pp. 2553–2558.
- [13] S. S. Christensen, R. Agarwal, E. De Carvalho, and J. M. Cioffi, "Weighted sum-rate maximization using weighted mmse for mimo-bc beamforming design," *IEEE Transactions on Wireless Communications*, vol. 7, no. 12, pp. 4792–4799, 2008.
- [14] Q. Shi, M. Razaviyayn, Z.-Q. Luo, and C. He, "An iteratively weighted MMSE approach to distributed sum-utility maximization for a MIMO interfering broadcast channel," *IEEE Transactions on Signal Processing*, vol. 59, no. 9, pp. 4331–4340, 2011.
- [15] K. Shen and W. Yu, "Fractional programming for communication systems—part I: Power control and beamforming," *IEEE Transactions on Signal Processing*, vol. 66, no. 10, pp. 2616–2630, 2018.
- [16] X. Zhao, S. Lu, Q. Shi, and Z.-Q. Luo, "Rethinking WMMSE: Can its complexity scale linearly with the number of BS antennas?" *IEEE Transactions on Signal Processing*, vol. 71, pp. 433–446, 2023.
- [17] K. Shen and W. Yu, "Fractional programming for communication systems—part II: Uplink scheduling via matching," *IEEE Transactions on Signal Processing*, vol. 66, no. 10, pp. 2631–2644, 2018. [Online]. Available: <https://arxiv.org/abs/1802.10197>
- [18] A. A. Khan, R. S. Adve, and W. Yu, "Optimizing downlink resource allocation in multiuser mimo networks via fractional programming and the hungarian algorithm," *IEEE Transactions on Wireless Communications*, vol. 19, no. 8, pp. 5162–5175, 2020.
- [19] H. Sun, X. Chen, Q. Shi, M. Hong, X. Fu, and N. D. Sidiropoulos, "Learning to optimize: Training deep neural networks for wireless resource management," *IEEE Transactions on Signal Processing*, vol. 66, no. 20, pp. 5438–5453, 2018.
- [20] L. Liang, H. Ye, G. Yu, and G. Y. Li, "Deep-learning-based wireless resource allocation with application to vehicular networks," *Proceedings of the IEEE*, vol. 108, no. 2, pp. 341–356, 2019.
- [21] A. Alwarafy, M. Abdallah, B. S. Ciftler, A. Al-Fuqaha, and M. Hamdi, "Deep reinforcement learning for radio resource allocation and management in next generation heterogeneous wireless networks: A survey," *arXiv preprint arXiv:2106.00574*, 2021. [Online]. Available: <https://arxiv.org/abs/2106.00574>
- [22] Y. Shen, Y. Shi, J. Zhang, and K. B. Letaief, "Lorm: Learning to optimize for resource management in wireless networks with few training samples," *IEEE Transactions on Wireless Communications*, vol. 19, no. 1, pp. 665–679, 2020.
- [23] W. Cui, K. Shen, and W. Yu, "Spatial deep learning for wireless scheduling," *IEEE Journal on Selected Areas in Communications*, vol. 37, no. 6, pp. 1248–1261, 2019.
- [24] Y. Shen, Y. Shi, J. Zhang, and K. B. Letaief, "Graph neural networks for scalable radio resource management: Architecture design and theoretical analysis," *IEEE Journal on Selected Areas in Communications*, vol. 39, no. 1, pp. 101–115, 2021.
- [25] Z. Wang, M. Eisen, and A. Ribeiro, "Learning decentralized wireless resource allocations with graph neural networks," *IEEE Transactions on Signal Processing*, vol. 70, pp. 1850–1863, 2022.
- [26] S. Lu, S. Zhao, and Q. Shi, "Learning-based massive beamforming," in *GLOBECOM 2020-2020 IEEE Global Communications Conference*. IEEE, 2020, pp. 1–6.
- [27] V. Monga, Y. Li, and Y. C. Eldar, "Algorithm unrolling: Interpretable, efficient deep learning for signal and image processing," *IEEE Signal Processing Magazine*, vol. 38, no. 2, pp. 18–44, 2021.
- [28] Q. Hu, Y. Cai, Q. Shi, K. Xu, G. Yu, and Z. Ding, "Iterative algorithm induced deep-unfolding neural networks: Precoding design for multiuser MIMO systems," *IEEE Transactions on Wireless Communications*, vol. 20, no. 2, pp. 1394–1410, 2021.
- [29] L. Pellaco, M. Bengtsson, and J. Jaldén, "Matrix-inverse-free deep unfolding of the weighted mmse beamforming algorithm," *IEEE Open Journal of the Communications Society*, vol. 3, pp. 65–81, 2021.
- [30] A. Chowdhury, G. Verma, A. Swami, and S. Segarra, "Deep graph unfolding for beamforming in MU-MIMO interference networks," *IEEE Transactions on Wireless Communications*, vol. 23, no. 5, pp. 4889–4903, 2024.
- [31] J. Zhu, T.-H. Chang, L. Xiang, and K. Shen, "Deepfp: Deep-unfolded fractional programming for mimo beamforming," *IEEE Transactions on Communications*, 2026.
- [32] Y. Sun, P. Babu, and D. P. Palomar, "Majorization-minimization algorithms in signal processing, communications, and machine learning," *IEEE Transactions on Signal Processing*, vol. 65, no. 3, pp. 794–816, 2017.
- [33] K. Shen, Z. Zhao, Y. Chen, Z. Zhang, and H. V. Cheng, "Accelerating quadratic transform and WMMSE," *IEEE Journal on Selected Areas in Communications*, vol. 42, no. 11, pp. 3110–3124, 2024.
- [34] J. Liu, X. Chen, Z. Wang, and W. Yin, "Alista: Analytic weights are as good as learned weights in lista," in *International conference on learning representations*, 2019.
- [35] C. Bertocchi, E. Chouzenoux, M.-C. Corbineau, J.-C. Pesquet, and M. Prato, "Deep unfolding of a proximal interior point method for image restoration," *Inverse Problems*, vol. 36, no. 3, p. 034005, 2020.
- [36] S. Mukherjee, A. Hauptmann, O. Öktem, M. Pereyra, and C.-B. Schönlieb, "Learned reconstruction methods with convergence guarantees: A survey of concepts and applications," *IEEE Signal Processing Magazine*, vol. 40, no. 1, pp. 164–182, 2023.
- [37] R. S. Sutton, D. McAllester, S. Singh, and Y. Mansour, "Policy gradient methods for reinforcement learning with function approximation," *Advances in neural information processing systems*, vol. 12, 1999.